https://doi.org/10.5194/egusphere-2026-1043
Preprint. Discussion started: 11 May 2026


# Lagrangian investigation of GCMs during the 2014-15 Holuhraun eruption reveals large differences in the representation of aerosol size distribution.

Eliza K. Duncan[1], George Jordan[2], Paul Kim[1], James M. Haywood[1], Duncan Watson-Parris[3], Ben Johnson[2], Alistair Sellar[4], Zak Kipling[5], João Teixeira[2], Florent Malavelle[4], and Daniel G. Partridge[1]

[1]Department of Mathematics and Statistics, University of Exeter, Exeter, EX4 4QF, United Kingdom
[2]Met Office Hadley Centre, Exeter, EX1 3PB, United Kingdom
[3]Scripps Institution of Oceanography and Halıcıoğlu Data Science Institute, University of California San Diego, California, CA 92093, USA
[4]Met Office, Exeter, EX1 3PB, United Kingdom
[5]European Centre for Medium-Range Weather Forecasts, Reading, RG2 9AX, United Kingdom

*Correspondence to*: Eliza K. Duncan (e.k.duncan@exeter.ac.uk) and Daniel G. Partridge (D.G.Partridge@exeter.ac.uk)

**Abstract.**

Our ability to understand and predict future climate scenarios remains limited by significant uncertainties in climate modelling, particularly those related to aerosol-cloud interactions (ACI). The Holuhraun eruption (2014-2015) provides an ideal opportunity to investigate ACI, with peak daily sulphur dioxide ($SO_2$) emission rates exceeding that of all anthropogenic sources in Europe. In this study we perform the first Lagrangian evaluation of aerosol processes associated with an effusive volcanic perturbation that combines in-situ aerosol particle number size distribution (PNSD) from rural in-situ sites with air mass back-trajectories to understand differences in general circulation model (GCM) representations. Holuhraun significantly impacted the observed PNSD at the three sites considered, showing a consistent increase in the accumulation modal diameter and evidence of sustained growth during transport from new particle formation (NPF) in the plume. ECHAM6.3-HAM2.3 did not replicate the observed sustained growth from NPF events, instead the volcanic perturbation was associated with growth of pre-existing particles, contributing to the mass of aerosol. Contrastingly, UKESM1.0 demonstrated no increase in the modal diameter during the eruption period. The inclusion of organic-mediated boundary layer nucleation (BLN) into UKESM1.0 (UKESM-BLN), enabled a considerably better representation of PNSD changes. UKESM-BLN replicated the increase in accumulation mode diameter, as well as sustained NPF events, although it considerably overestimated number concentrations of Aitken mode particles. Investigating the perturbation in cloud condensation nuclei during the eruption year demonstrated that UKESM-BLN better replicated the perturbation at the boreal sites, highlighting the importance of BLN processes in accurate representation of ACI in GCMs.

https://doi.org/10.5194/egusphere-2026-1043
Preprint. Discussion started: 11 May 2026


## 1. Introduction

Aerosol-cloud interactions (ACI) remain one of the largest sources of uncertainty in climate modelling. Significant differences persist in the magnitude in climate model response to aerosol forcing (Ghan et al., 2016). Volcanic eruptions offer opportunistic natural experiments to investigate ACI (Christensen et al., 2022). In particular, the Holuhraun effusive eruption (64.85°N, 16.83°W) provides an ideal opportunity to investigate ACI, with peak daily $SO_2$ emission rates three times that of all anthropogenic sources in Europe (Schmidt et al., 2015) that affected a relatively pristine environment in the North Atlantic. The eruption began on the 31st of August 2014 and continued until 28th of February 2015 (Schmidt et al., 2015; Sigmundsson et al., 2015) and was the largest effusive eruption in Iceland since the 1783-1784 Laki eruption (Ilyinskaya et al., 2017). Several previous studies have used Holuhraun as an opportunity to investigate ACI (Chen et al., 2022; McCoy and Hartmann, 2015; Zoëga et al., 2025a, b) and ACI representation by GCMs (e.g. Haghighatnasab et al., 2022; Jordan et al., 2024; 2025; Malavelle et al., 2017; Peace et al., 2024). Jordan et al. (2025) isolated the aerosol effect from the meteorological variability and found that GCMs were able to capture the observed cloud microphysical changes associated with the ACI first indirect effect in the plume over the North Atlantic, but the magnitude of the response varied between models and they found large differences in the climatological baseline of cloud droplet number concentration (CDNC). The CDNC perturbation associated with the eruption will be strongly affected by the baseline aerosol state (Carslaw et al., 2013; Marelle et al., 2025), which motivates accurate characterisation of the particle number size distribution (PNSD) by GCMs.

Many studies have looked at the second indirect effects associated with the Holuhraun eruption. Malavelle et al. (2017) and Peace et al. (2024) used the Holuhraun eruption to demonstrate that there was little if any impact on the cloud liquid water path in satellite observations. Chen et al. (2022) used a machine learning approach trained on long-term satellite observations to demonstrate that the cloud fraction was significantly enhanced during the eruption. Increased liquid water path and cloud fraction in the Arctic associated with the Holuhraun eruption was found to lead to surface warming through trapping of longwave radiation (Zoëga et al., 2025a). The majority of climate models were not able to capture the second indirect effects (e.g. Jordan et al., 2025), although higher resolution modelling studies show better agreement with satellite observations (Haghighatnasab et al., 2022; Yoshioka et al., 2025). However, previous studies have not interrogated the process scale chain from emission to ACI, to identify relative importance of aerosol lifecycle processes attributable to differences in GCM response in cloud condensation nuclei (CCN).

To fully assess GCMs ability to model ACI, it is necessary to examine the full pathway of particle formation and growth, starting from the oxidation of emitted $SO_2$ through to the subsequent growth of aerosol to CCN sizes. $SO_4$ is produced from $SO_2$ following two distinct pathways: in-cloud and out-of-cloud oxidation. Out-of-cloud oxidation refers to the gas phase in which $SO_2$ oxidation mainly occurs through reactions with hydroxyl radicals (OH), forming sulphuric acid (gas) (Stockwell and Calvert, 1983). Hygroscopic sulphuric acid can condense onto existing particles (Seinfeld and Pandis, 2006) or can nucleate to form new particles in volcanic plumes (Boulon et al., 2011; Twigg et al., 2016). Aqueous phase oxidation occurs

https://doi.org/10.5194/egusphere-2026-1043
Preprint. Discussion started: 11 May 2026


much faster through heterogenous reactions with dissolved ozone and hydrogen peroxide ($H_2O_2$) in clouds (e.g. Calvert et al., 1978), with the reaction rates being dependent on pH (Seinfeld and Pandis, 2006, eq. 6.86). Aqueous phase oxidation occurs on timescales of hours or days, and results in larger particles than gas-phase oxidation, which occurs on timescales of days to weeks (Faloona, 2009; von Glasow et al., 2009). The oxidation rates and relative contribution of the two phases is uncertain and can result in significantly different physical and chemical properties of aerosol particles and are important to constrain in GCMs to accurately represent CCN and therefore ACI (Goto et al., 2011; Jordan et al., 2024).

Studies have investigated the plume characteristics of the Holuhraun eruption using ground-based measurements and trajectory modelling with reanalysis data to attribute pollution events to the eruption (Schmidt et al., 2015; Twigg et al., 2016) and estimate the oxidation rates from $SO_2$ to $SO_4$ (Boichu et al., 2019; Ilyinskaya et al., 2017). Jordan et al. (2024) performed a model evaluation study, investigating the representation of the evolution of the plume and production of sulphate across 6 numerical models. They found that the derived oxidation rate constants were lower than the observed rate, suggesting the representation of the oxidation pathways results in too slow conversion in the simulated plumes. Improving understanding of the drivers of uncertainty in these pathways and their associated impact on the production of sulphate aerosol in GCMs is important for constraining ACI as sulphate particles have been shown to grow to CCN sizes during the Holuhraun eruption through new particle formation (NPF) (Twigg et al., 2016).

A Lagrangian framework enables novel evaluation of GCM outputs in which the evolution of aerosols and other variables is followed over both time and space to facilitate more rigorous observational constraints compared to traditional Eulerian approaches, to be able to identify the sources of differences in the GCMs. To achieve this, we employ a recently developed Lagrangian framework (Kim et al., 2020; Talvinen et al., 2025) to investigate the differences in aerosol representation in two GCMs. This provides additional insight into the representation of the aerosol lifecycle during transport by incorporating GCM fields with air-mass trajectories driven by GCM output. Using in-situ ground-based measurements from sites in the Arctic and boreal forest, we evaluate how well the models capture perturbations in aerosol properties during the eruption period. We perform the analysis during September 2014 when the gaseous $SO_2$ emissions were most intense (Carboni et al., 2019), affecting many surface air quality observation sites across Europe (Boichu et al., 2019; Jordan et al., 2024, 2025; Schmidt et al., 2015; Twigg et al., 2016).

This work achieves the following, we:-

1. Evaluate the GCM representation of the aerosol perturbation from the Holuhraun plume in both Eulerian and Lagrangian frames of reference.
2. Investigate the mechanisms leading to sulphate aerosol production and the differences between GCMs.
3. Investigate the potential impact on cloud properties.

https://doi.org/10.5194/egusphere-2026-1043
Preprint. Discussion started: 11 May 2026


This paper is structured as follows: Sect. 2 describes the datasets and methodology; the results for the Eulerian and Lagrangian GCM evaluations are presented and discussed in Sect. 3 and Sect. 4 respectively, and the conclusions are reviewed in Sect. 5.

95

https://doi.org/10.5194/egusphere-2026-1043
Preprint. Discussion started: 11 May 2026


## 2. Datasets and Methodology

Several different datatypes are used in this study: in-situ observations, ERA-Interim reanalysis data, GCM outputs and Hybrid Single Particle Lagrangian Integrated Trajectory (HYSPLIT) model trajectories. In this section we describe the datasets, model simulations and any processing applied.

### 2.1 In-situ observations

Rural ground-based measurement sites across Europe were used to obtain aerosol size distribution data from DMPS (Differential Mobility Particle Sizer) measurements. Sites were selected from the ACTRIS (Aerosol, Clouds and Trace gases Research InfraStructure) network (Laj et al., 2024) based on three key criteria:

1. Surface station must have experienced the volcanic plume and sample aerosol particle size distribution at least at 3-hourly resolution during September 2014 to collocate to hourly resolution trajectories in a statistically robust way and facilitate analysis of the spatial evolution of the aerosol population at a high temporal resolution.
2. A long-term series of measurements is available at the surface stations to provide a climatology for comparison against which volcanic influences can be compared.
3. A location for which transport pathways can be selected to isolate the impact of the volcano, and without significant local urban pollution.

Three sites were found to match these criteria (Fig. 1). The first site, Värriö (VAR) SMEAR I station is located 120km north of the Arctic circle in the Finnish boreal forest (67.767°N, 29.583°E, 390m a.s.l.) (Hari et al., 1994). The site is in a strictly enforced nature reserve with practically no local pollution at the site, the nearest village (Savukoski) is 100 km away (Vehkamäki et al., 2004). 250km West of Värriö is Pallas (Sammaltunturi) (PAL) (67°58 N, 24°06 E, 565 m asl.) (Hatakka et al., 2003), part of the Global Atmosphere Watch programme. For the northernmost site, we use measurements from the Zeppelin Mountain station (ZEP) (78.906ºN, 11.888ºE, 472m a.s.l.) in the remote arctic environment on Svalbard (Ström et al., 2003). The time-period and size ranges used for each station are described in Table 1. Pallas (Matorova, within 12km of Sammaltunturi) provides sulphur dioxide measurements from Filter-3 pack instruments during the eruption period on a daily resolution, thus all datasets used for sulphur dioxide concentrations are averaged to daily concentration, using the mean, to facilitate comparison. The Zeppelin Mountain station was closed due to maintenance mid-July to early October in 2014 so there were no Filter-3pack measurements for September 2014, however there was a $SO_2$ monitor in nearby Ny-Ålesund during this period which we included to facilitate an estimation of volcanic influence near Zeppelin.

https://doi.org/10.5194/egusphere-2026-1043
Preprint. Discussion started: 11 May 2026


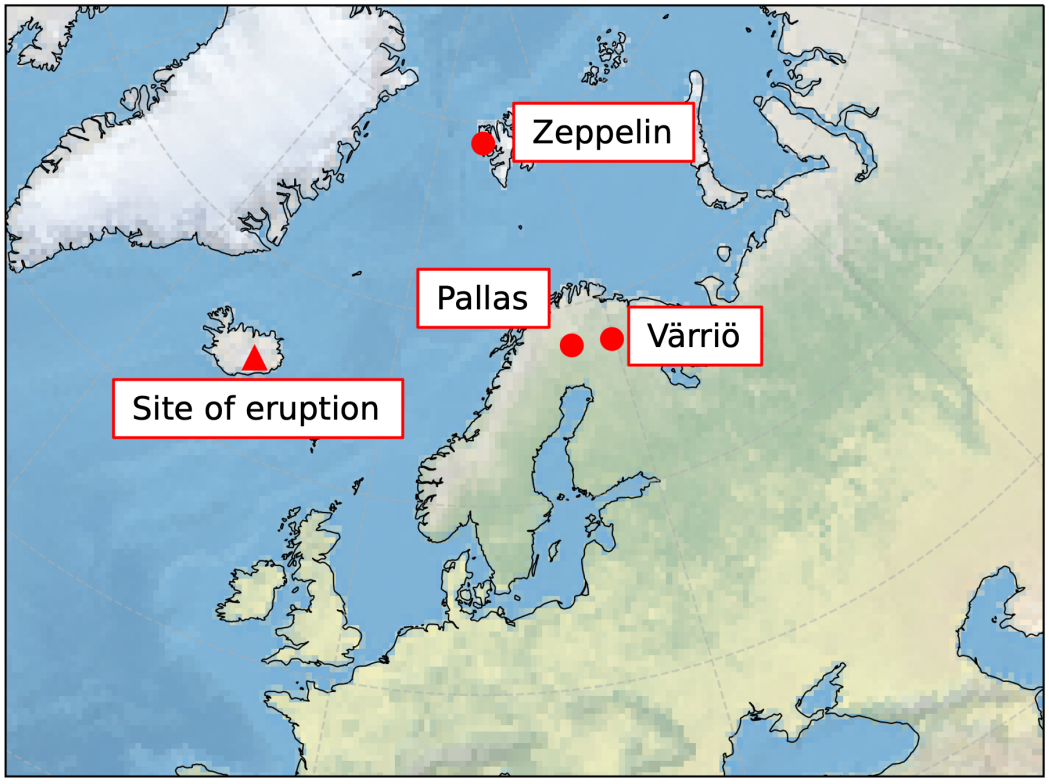


**Figure 1: A map of the selected stations (Värriö (Finland), Pallas (Finland) and Zeppelin (Norway)) and site of eruption (Holuhraun, Iceland). Map source: Natural Earth.**

### 2.2 In-situ data processing

To ensure consistency across sites and years, a data driven filtering approach was applied, with four additional filters applied to the ACTRIS DMPS size distribution data after any flagged (EBAS Data Submission Manual, 2025) distributions are removed, to reject any distributions with significant missing data as well as significant outliers. Considering groups of consecutive missing data points in each particle number distribution, a distribution is excluded from analysis if the difference in the logarithm of the distribution bin midpoint diameters ($dlogD_p$) of the consecutive bins exceeds 0.1. Distributions are also excluded if the percentage of missing values exceeds 10% of the number of bins in the distribution. We also remove any outlier distributions that exceed a total concentration threshold of 99.5% over the years used in this study (2009-2014 for Värriö and Pallas and 2010-2014 for Zeppelin). The largest two bins at the detection limit of the instrument also have a 99.5% outlier threshold applied. The filtering results are shown in Table S3 to S5.

To maintain consistency across instruments at the sites and ensure comparability with GCM data, a common grid of bin diameter midpoints is defined. This grid is defined over 1-1000nm which spans over the range for the instruments used for all

https://doi.org/10.5194/egusphere-2026-1043
Preprint. Discussion started: 11 May 2026


stations. Note that the DMPS measurements fall within this range and we do not extrapolate beyond the measurement limits. Measurements in the sub-10 nm range are subject to very high counting uncertainties due to high particle losses and are often derived from only a few counts in DMPS measurement systems (Stolzenburg et al., 2023), thus we did not focus on the sub-10nm range in this study. Therefore, observations of the nucleation mode, defined as 1-10nm in this study, are not included in the analysis for the observations and we initiate any integration over the size ranges from 10nm for all datasets. We define the Aitken mode as 10-100nm, the accumulation mode as 100nm to the instrument limit at the site (Table 1) and the total concentration as 10nm to instrument limit at the site (Table 1). We utilise a $dlogD_p$ of 0.015 which results in a resolution of 200 bins. The Piecewise Cubic Hermite Interpolating Polynomial (PCHIP) function (Fritsch and Butland, 1984) from the SciPy package (Virtanen et al., 2020) is used to interpolate the PNSD to the common grid, the considerations for utilising the PCHIP algorithm for interpolation of PNSD are discussed in Duncan et al. (2025). This method of interpolation results in negligible differences of the total concentration where the bin midpoints of the new and original grid do not match (Fig. S1). After filtering and interpolation, timesteps are then selected to match the three-hour resolution of the GCM output, due to the importance of temporal collocation for model evaluation, which is discussed, for example, in Schutgens et al. (2016).

### 2.3 Numerical model simulations

The models used in this study are UKESM1.0, and ECHAM6.3-HAM2.3 which participated in the AEROCOM II VolcACI (Jordan et al., 2024, 2025) and GCMTraj experiments (Kim et al., 2020; Talvinen et al., 2025). Simulations are performed in the atmosphere-only configuration (AMIP-style) and use monthly observational datasets to prescribe sea surface temperature and sea ice boundary conditions as described in Sellar et al. (2020). The simulations are nudged to ERA-Interim reanalysis (Dee et al., 2011) of horizontal wind speeds, generally above the boundary layer, at a 6-hourly resolution. The horizontal winds are not nudged at all model levels; the lowermost levels are excluded to minimise impact from the boundary layer. Nudging only the horizontal winds, not potential temperature provides a well constrained meteorology, but without strongly perturbing the mean climate which is important for cloud feedbacks (Zhang et al., 2014). Simulations are conducted in the native resolutions: 1.25°×1.875° with 85 vertical levels (UKESM1.0) and 1.875°×1.875° with 47 vertical levels (ECHAM6.3-HAM2.3).

UKCA (the UK Chemistry and Aerosol model) is the coupled aerosol and chemistry model used to simulate aerosols in UKESM1.0, whereas ECHAM6.3 uses the HAM2.3 model. Both aerosol schemes use a log-normal pseudo-modal scheme and include the processes of nucleation, condensation, growth, coagulation, wet and dry deposition, and cloud processing (Spracklen et al., 2005; Stier et al., 2005). UKCA uses a two-moment dynamic approach (the mass and number in each mode) (Mann et al., 2010). For the UKESM set-up, an insoluble Aitken mode and 4 soluble size modes are used, described in the supplementary material, Table S6, within which aerosol mass is broken into internally mixed modes for the calculation of aerosol mass. In UKESM, mineral dust aerosol is simulated independently of the other aerosol species using the CLASSIC dust scheme (Bellouin et al., 2011; Mulcahy et al., 2020). HAM similarly uses a two-moment dynamic aerosol scheme but

https://doi.org/10.5194/egusphere-2026-1043
Preprint. Discussion started: 11 May 2026


uses 4 soluble size modes and 3 insoluble (Aitken, accumulation and coarse) as standard (Tegen et al., 2019) (described in Table S7).

ECHAM6.3-HAM2.3 includes an organic-mediated scheme for boundary layer nucleation over forest as well as neutral and charged nucleation of sulphuric acid throughout the troposphere (Zhang et al., 2012) whereas UKESM1.0 as standard only includes neutral binary homogenous nucleation throughout the troposphere (Mulcahy et al., 2020). In addition to the standard UKESM1.0 setup, a simulation was conducted including organic-mediated nucleation in the boundary layer using the Metzger et al. (2010) parameterisation, which has been found in previous studies to give much better agreement with observations (Ranjithkumar et al., 2021). The boundary layer nucleation (BLN) rate for this parameterisation was reduced by a factor of 10 as this was found to reduce bias in the boundary layer of total aerosol concentration by ~67% (Ranjithkumar et al., 2021). Simulations for the configuration of UKESM1.0 with boundary layer nucleation (UKESM-BLN), were conducted in an identical manner to UKESM1.0. These GCM simulations will be referred to by the abbreviations UKESM, UKESM-BLN and ECHAM hereafter.

The simulations of the eruption at Holuhraun in 2014 use emission altitude and magnitude described by Malavelle et al. (2017), distributed between the 800m and 3000km in the grid-cell of the fissure. The absolute fraction of $SO_2$ emitted as primary $SO_4$ is 0.025, emitted into the soluble Aitken and accumulation modes with a mean radius of $0.0525\mu m$. Control runs were also conducted for 2009-2013 which do not include any volcanic emissions from Holuhraun. Size distributions are calculated from the modal aerosol outputs linearly interpolated to the latitude, longitude and height of the aerosol measurement "receptor" sites (described further in Sect. 2.5), on the 1-1000nm grid of the ACTRIS observations (see Sect. 2.2) for consistency using the 3-hourly model instantaneous outputs.

### 2.4 Air-mass back trajectories

To investigate the life cycle of aerosol during transport, air-mass back trajectories were calculated using the Hybrid Single Particle Lagrangian Integrated Trajectory (HYSPLIT) model (Stein et al. 2015). The HYSPLIT version used in this study (5.1.0 revision 1639) includes a minor bugfix to improve the velocity interpolation calculation of trajectories passing near the poles (personal correspondence, Alice Crawford, NOAA). For each in-situ measurement site, 240-hourly backwards trajectories were initiated at each 3-hourly time point (corresponding to GCM model output resolution). Trajectories were calculated using 6-hourly (1.0°×1.0°) ERA-Interim reanalysis data as well as 3-hourly data from UKESM, UKESM-BLN and ECHAM. ERA-Interim was used as the reanalysis dataset to facilitate comparison to the GCM simulations which were nudged to ERA-Interim wind fields. The meteorological fields from the GCMs were first re-gridded onto a consistent 1.0°×1.0° grid netCDF4 format, then converted into the Air Resources Laboratory (ARL) packed HYSPLIT compatible format (Kim et al., 2020). For ECHAM the output was provided on terrain-following model levels for the vertical grid. In UKESM the native output is on hybrid height levels, for use with HYSPLIT UKESM data was instead output on fixed pressure levels which

https://doi.org/10.5194/egusphere-2026-1043
Preprint. Discussion started: 11 May 2026


closely match the vertical coordinates of ERA-Interim (Talvinen et al., 2025). Trajectory release points for each site are described in Table 1. The trajectories were initialised at a minimum height of 100 m above ground level (a.g.l.), and to account for the difference between the orography at the site and the orography represented in the dataset an average offset was approximated for each site (Table S8).

To account for the uncertainty of single-particle trajectories, which is thought to be dominated by the underlying meteorology (e.g. Engström & Magnusson, 2009), due to the shorter analysis period associated with the eruption we utilise an ensemble of trajectories (Stein et al., 2015) for all calculations. The meteorological dataset is perturbed by a fixed grid factor of 1.0 degree in the horizontal (for both latitude and longitude) and 0.01σ units in the vertical, resulting in a 27-member ensemble, initiated in a 3-dimensional cube centred around the receptor starting point.

https://doi.org/10.5194/egusphere-2026-1043
Preprint. Discussion started: 11 May 2026


210

| Station | Time period | Aerosol size distribution bin midpoint diameters ($D_p$) range used in this study | Aerosol environment description | Trajectory release location | | |
|---|---|---|---|---|---|---|
| | | | | Latitude (decimal) | Longitude (decimal) | Height (m a.g.l.) |
| Värriö | September 2009-2014 | 10-790nm | Boreal (rural) (Hari et al., 1994) | 67.767 | 29.583 | 150 |
| Pallas | September 2009-2014 | 10-430nm | Boreal (rural) (Hatakka et al., 2003) | 67.973 | 24.116 | 200 |
| Zeppelin | September 2010-2014 | 10-630nm | Arctic (rural) (Ström et al., 2003) | 78.906 | 11.888 | 350 |

**Table 1: The selected receptor sites with the years included in the study, aerosol size distribution bin midpoint diameters ($D_p$) range used in this study, the site description, and the trajectory release locations.**

### 2.5 Collocation

215 For Lagrangian analysis with the GCMs, we collocate variables along trajectories using linear interpolation. For ECHAM, variables are on a pressure grid, therefore variables are collocated to the relevant pressure, latitude and longitude of the trajectory points, whereas UKESM data is output on model levels, therefore the data is interpolated to the height above ground (and latitude and longitude) of the trajectories. The collocated GCM variables include lognormal aerosol size distribution modal parameters (Tables S6 and S7), air density and $SO_2$ and $SO_4$ mass mixing ratios. Collocation of datasets onto trajectories
220 is performed for the GCMs using a collocator tool (Kim et al., 2020) based on the Community Intercomparison Suite (CIS, Watson-Parris et al., 2016). Selected variables are collocated onto trajectories in 4 dimensions (model/ pressure level, latitude, longitude, and time) using linear interpolation over rectilinear grids provided by the SciPy library (Virtanen et al., 2020). Near the surface when linear interpolation would result in a missing value, nearest-neighbour interpolation is applied instead, avoiding extrapolation outside of the data domain (Talvinen et al., 2025). The PNSD for each trajectory timestep is calculated
225 on the same size grid as the observations (Sect. 2.2) from the collocated log-normal modal parameters. For comparison with the in-situ observations in the Eulerian analysis (Sect. 3), the median is taken across the collocated ensemble of trajectories at the first timestep of the backwards trajectories (the starting point at the measurement receptor site location) for the GCM

https://doi.org/10.5194/egusphere-2026-1043
Preprint. Discussion started: 11 May 2026


diagnostic outputs: PNSD (derived from lognormal parameters described in table S6 and S7), $SO_2$ mass mixing ratio and density of air. The $SO_2$ mass concentration is then calculated from the $SO_2$ mass mixing ratio and density of air.

230

### 2.6 Receptor models

Three types of receptor models are used in this study to inform our understanding of the difference between GCM simulated and observed properties of the aerosol PNSD during the Holuhraun eruption. Each of these receptor models are obtained consistently using air-mass trajectories derived from both ERA-Interim reanalysis and GCM meteorological driving datasets.

235 First, transport frequency receptor models are used to investigate the spatial distribution of the airmass history for each site. This is defined over a grid for longitude $i$ and latitude $j$, with the frequency of transport within a given grid cell defined as:

$$F_{ij} = \frac{100}{T}\sum_{l=1}^{M} v_{ijl} \quad (1)$$

where $F_{ij}$ is the frequency of visits for a grid cell, $T$ is the total number of trajectories, $v_{ijl}$ the number of unique visits by a trajectory, $l$, in the grid cell, $i, j,$ and $M$ is the total number of trajectories with endpoints in the $i, j$th grid cell.

240 Concentration weighted trajectory (CWT) receptor models are used to investigate the potential dominant sources of aerosols for each receptor site used in this study. These are defined over the same grid as in Eq. 1, using the definition in Hsu et al. (2003):

$$C_{i,j} = \frac{1}{\sum_{l=1}^{M}\tau_{ijl}}\sum_{l=1}^{M} C_l\tau_{ijl} \quad (2)$$

where $C_l$ is the concentration measured at the 'receptor' site associated with trajectory $l$, $\tau_{ijl}$ is the total number of trajectories
245 endpoints in the grid cell $(i, j)$ associated with the $C_l$ sample.

Collocated variable trajectory (CVT) receptor models represent an average of a collocated variable at a point in space during the transport of the airmass to the measurement site. Similarly to the meteorological weighted trajectory models in Pernov et al. (2024), this will closely reflect the monthly mean distribution for the collocated values but considers the spatial variability in meteorological conditions and air mass transport pathways (Pernov et al., 2024). The CVT receptor model is described by
250 equation 3:

$$V_{i,j} = \frac{1}{\sum_{l=1}^{M}\tau_{ijl}}\sum_{l=1}^{M} v_{ijl}\tau_{ijl} \quad (3)$$

https://doi.org/10.5194/egusphere-2026-1043
Preprint. Discussion started: 11 May 2026


where $v_{i,j,l}$ is the variable value associated with trajectory point, $\tau_{ijl}$, in the grid cell i, j is the total number of trajectories endpoints in the grid cell $(i, j)$.

A mask is applied to all the receptor models in this study, using the frequency transport model to mask any grid cells with fewer than the 10$^{th}$ percentile of trajectory counts.

### 2.7 Clustering

Trajectories were clustered based on latitude, longitude and height to isolate transport associated with the eruption using KMeans from the Python SciPy package. Clustering was conducted on the entire trajectory timeseries (September 2009-2014 for Pallas and Värriö, September 2010-2014 for Zeppelin) for all ensemble ERA-Interim trajectories, thus facilitating a comparison of the same transport pathways when considering climatology compared to volcano period (see Sect. 3.3). Before clustering, the latitude, longitude and altitude were converted to the Earth-Centred, Earth-Fixed (ECEF) cartesian coordinate system, to ensure all variables were on the same scale for clustering. The optimal number of clusters was selected based on the rate of decrease in within-cluster sum of squares. Five clusters were selected (Sect. S1.5) to represent the 3D transport pathways to each measurement site (Figs. 2, 3 and 4). These were used to index size distributions for both observations and GCMs to produce a consistent comparative dataset.

https://doi.org/10.5194/egusphere-2026-1043
Preprint. Discussion started: 11 May 2026


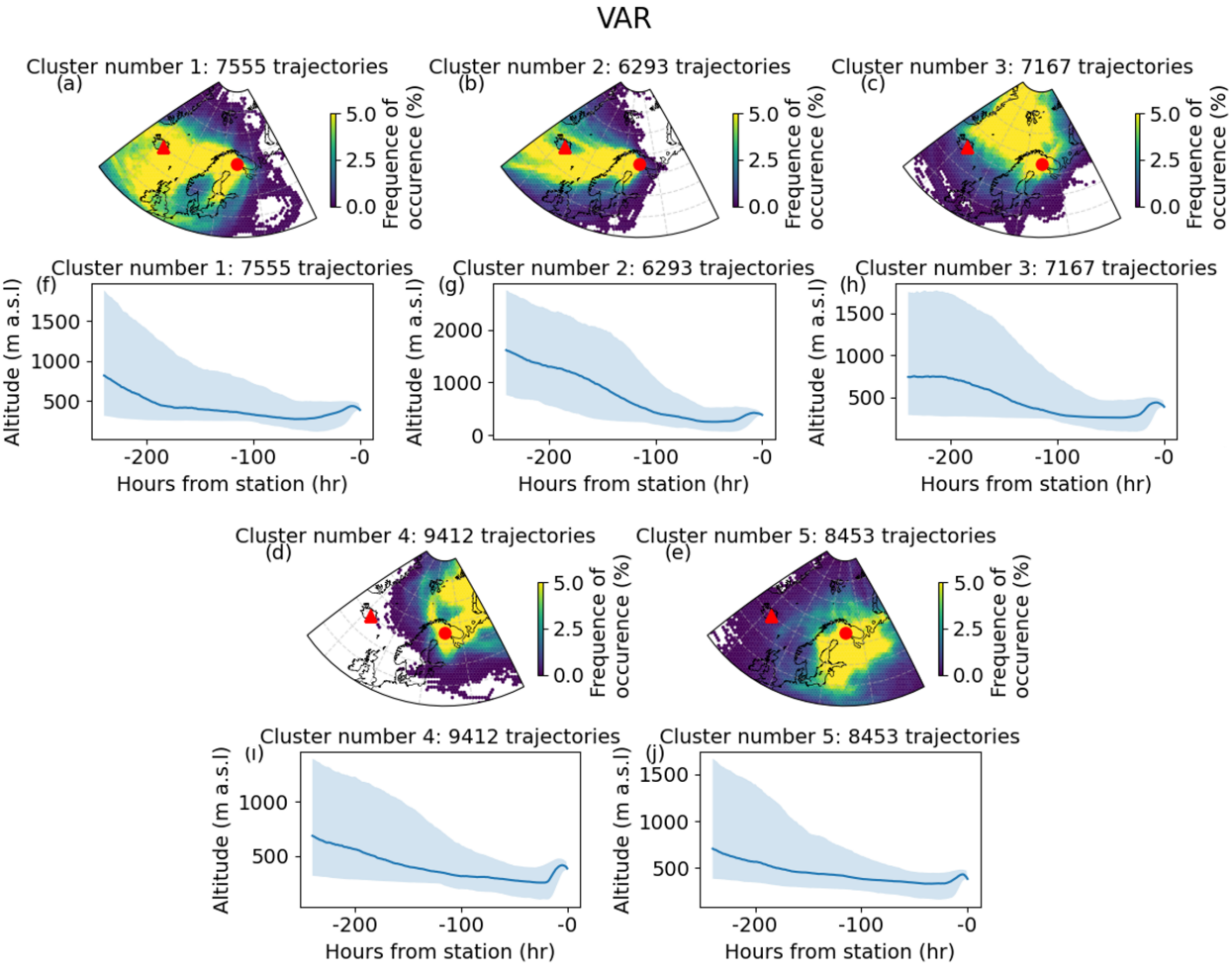


**Figure 2: (a-e) Transport frequency receptor models defined relative to the number of trajectories in each cluster, $F_{ij}$ as given by Eq. 1. (f-j) The median altitude for the trajectories in the cluster with the 25$^{th}$-75$^{th}$ percentiles indicated by the shaded area. For back-trajectories initiated at Värriö (Finland) indicated by the red circle. The eruption site at Holuhraun is indicated by the red triangle.**

https://doi.org/10.5194/egusphere-2026-1043
Preprint. Discussion started: 11 May 2026


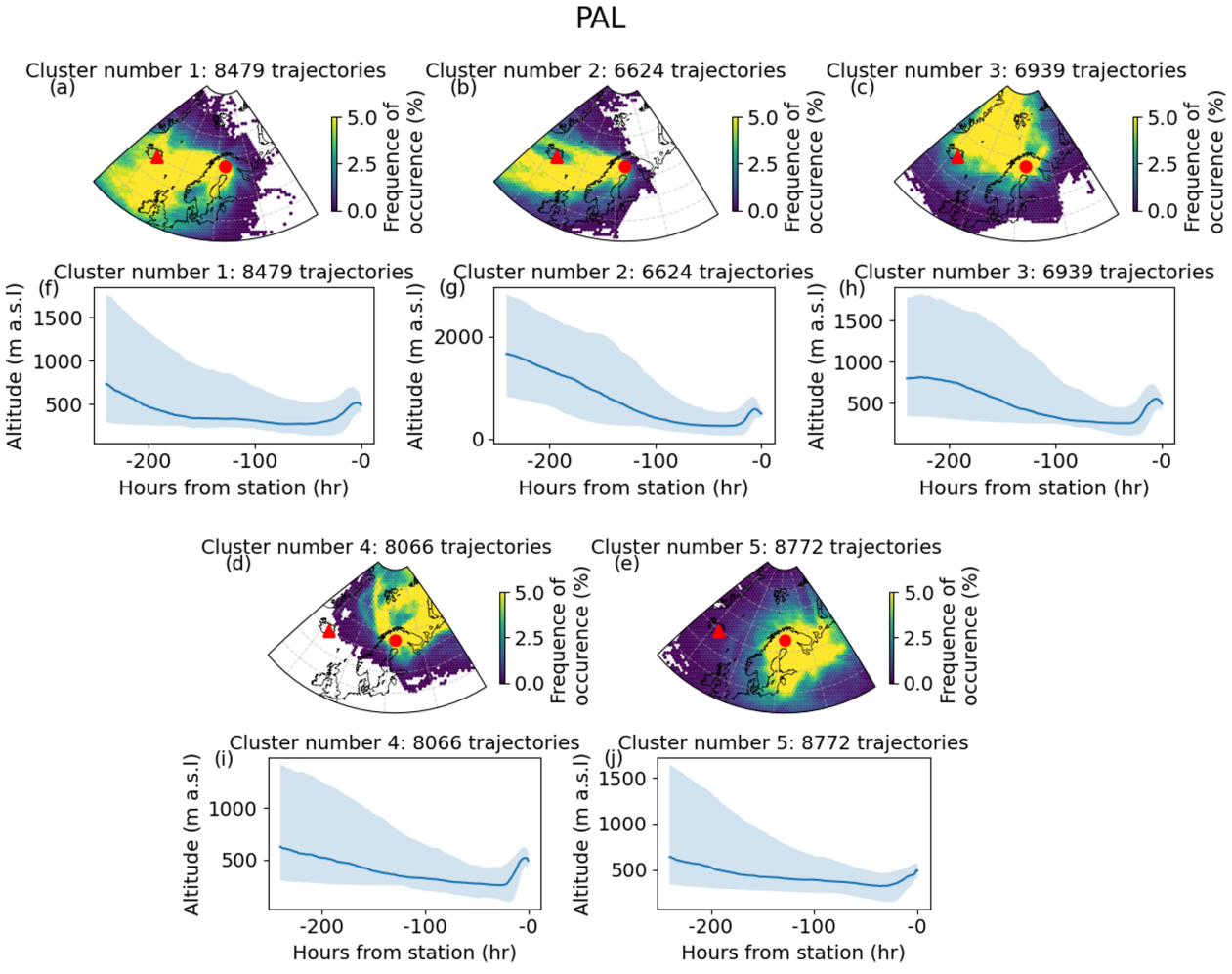


**Figure 3: (a-e) Transport frequency receptor models for each cluster, $F_{ij}$ as given by Eq. 1. (f-j) The median altitude for the trajectories in the cluster with the 25$^{th}$-75$^{th}$ percentiles indicated by the shaded area. For back-trajectories initiated at Pallas (Finland) indicated by the red circle. The eruption site at Holuhraun is indicated by the red triangle.**

280

https://doi.org/10.5194/egusphere-2026-1043
Preprint. Discussion started: 11 May 2026


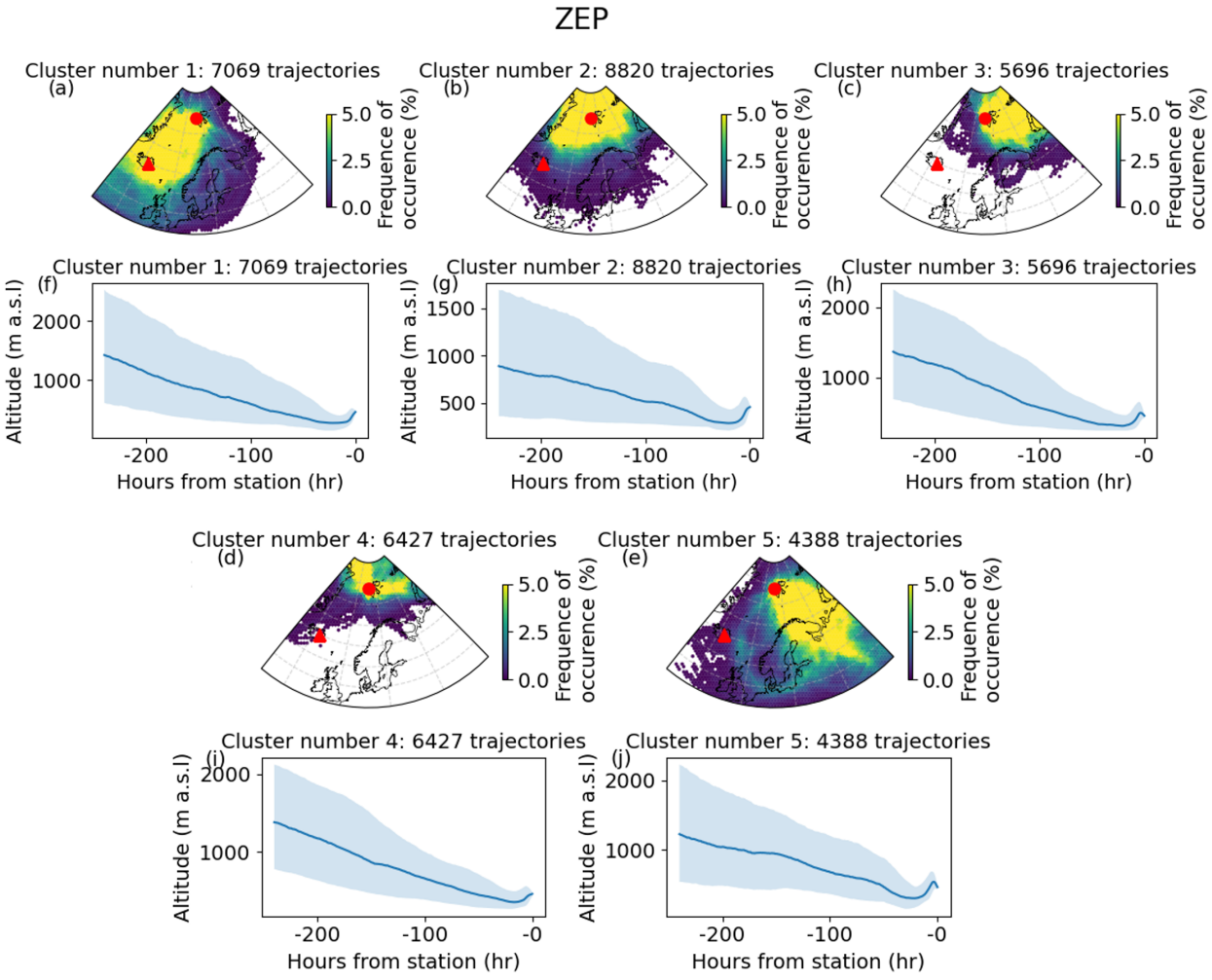


**Figure 4: (a-e) Transport frequency receptor models for each cluster, $F_{ij}$ as given by Eq. 1. (f-j) The median altitude for the trajectories in the cluster with the 25th-75th percentiles indicated by the shaded area. For back-trajectories initiated at Zeppelin (Svalbard) indicated by the red circle. The eruption site at Holuhraun is indicated by the red triangle.**

Värriö and Pallas exhibit very similar transport clusters (Figs. 2 and 3), which is expected due to the proximity of the two sites. We note that the main source of divergence between the cluster sets, is the altitude, where Pallas exhibits a more distinct 'peak' in most clusters close to the site. This is likely associated with airmasses rising and descending again over mountains, to which Pallas is closer in proximity than Värriö. The clustering results facilitate isolation of transport influenced by the eruption to the receptor sites for the Eulerian GCM evaluation. Clusters were selected that contain significant transport from the region of the eruption and are described in Table 4. These clusters were used to give the percentage of trajectories in volcanically influenced clusters for the Eulerian $SO_2$ (Sect. 3.1) and NMBF (Sect 3.2). The selected clusters were also used in the average size distribution analysis (Sect. 3.3) where size distributions filtered for transport from the eruption site for both the volcanic

https://doi.org/10.5194/egusphere-2026-1043
Preprint. Discussion started: 11 May 2026


and climatology period. Note that the use of ensemble trajectories (27 for each 3-hourly aerosol measurement timestep) means that multiple trajectories correspond to the same observation datapoint in time at the measurement sites. Thus, the number of trajectories associated with the selected clusters acts as weighting for the percentage of transport associated with the eruption for a datapoint when the median size distribution is calculated.

| Station | Selected clusters | Total number of trajectories in selected clusters |
|---|---|---|
| Värriö | 1, 2 | 13848 |
| Pallas | 1, 2 | 15103 |
| Zeppelin | 1 | 7069 |

**Table 4:** Selected clusters for each site and the total number of trajectories pre-aerosol filtering.

### 2.8 Normalised mean bias factor

The normalised mean bias factor (NMBF) is a symmetric unbiased metric of model performance defined in Yu et al. (2006). NMBF is used in this study to evaluate the performance of the GCMs compared to the observations for the for Aitken, accumulation and total number concentrations over the corresponding diameters. The NMBF is calculated for each day, to produce a time series, as well as across the month of September. The NMBF is defined as:

$$NMBF = \begin{cases} \frac{\sum M_i}{\sum O_i} - 1 = \frac{\bar{M}}{\bar{O}} - 1, & \bar{M} \geq \bar{O} \\ 1 - \frac{\sum O_i}{\sum M_i} = 1 - \frac{\bar{O}}{\bar{M}}, & \bar{M} < \bar{O} \end{cases} \quad (4)$$

where $M$ indicates the model and $O$ the observation. A positive NMBF indicates that the model prediction is higher than the observations, and a negative NMBF indicates that the model is lower than the observations. The magnitude of the model bias is given by 1+|NMBF|, which quantifies the factor by which the model underpredicts or overpredicts the observations.

### 2.9 Condensation sink

To investigate the aerosol processes, particularly NPF, the condensation sink was calculated which provides a measure of how rapidly condensable vapour molecules and newly formed molecular clusters are removed by the existing aerosol surface area. The condensation sink refers to the rate at which condensable gases condense onto aerosol particles in the atmosphere, defined as:

https://doi.org/10.5194/egusphere-2026-1043
Preprint. Discussion started: 11 May 2026


$$CS = 2\pi D \sum_j \beta_j d_j N_j \quad (5)$$

where D is the diffusion coefficient, $\beta_j$ is the transition regime correction factor (Fuchs and Sutugin, 1971), $d_j$ is the particle diameter and $N_j$ is the particle number concentration for the jth aerosol mode. We calculate the condensation sink utilising the method employed in Ranjithkumar et al., (2021), which follows the method employed in UKESM1.0. We assume sulphuric acid as the condensable vapour molecule.

https://doi.org/10.5194/egusphere-2026-1043
Preprint. Discussion started: 11 May 2026


## 3 Eulerian GCM evaluation

Firstly, we conducted a Eulerian evaluation of the impact of the volcanic eruption on the surface measurement sites and the representation of the perturbation in the GCMs, using GCM variables collocated to the trajectory starting points at the measurement sites.

### 3.1 $SO_2$ timeseries

To investigate the impact of the eruption on the selected measurement sites and the GCMs' ability to replicate the timing of the observed peak in $SO_2$, the timeseries of $SO_2$ concentrations measured at the eruption site during September 2014 was analysed (Fig. 5). Note that there were no observations of $SO_2$ at Värriö during this period, however the proximity of Pallas means that the timing of experienced $SO_2$ peaks was likely similar. We note that the peak in UKESM on the 16th of September at Värriö (Fig. 5a) is nearly absent in Pallas (Fig. 5b), indicating some divergence in the airmasses reaching the two sites at that time.

The percentage of trajectories for each day associated with the clusters defined as transport that would have been volcanically influenced for each site in Sect. 2.7 indicated by the red bars are mostly consistent between Värriö and Pallas. On the 10th of September when the $SO_2$ concentrations are at a peak at Pallas, we see a change in airmass direction to high percentages of volcanically influenced transport. Generally, the peaks in $SO_2$ coincide with higher percentages of transport from the region of the eruption. However, we note that the magnitude of the peaks in $SO_2$ does not correspond to the percentage of transport from the volcano, as this will depend on the conversion to $SO_4$ and loss during transport so is dependent on the time taken from the eruption as well as the meteorological conditions experienced during transport. There is a break in transport from the volcano during the third week for all sites, which corresponds to the changes in transport patterns found in Peace et al. (2024), considering transport over the North Atlantic.

Generally, the timings of the peaks are replicated well by UKESM, however the magnitude is notably lower (Fig. 5). The concentrations of UKESM-BLN are almost identical to those of UKESM, suggesting that boundary layer nucleation does not play a role in determining the $SO_2$ concentrations reaching the measurement site, which is consistent with results in Ranjithkumar et al. (2021), finding that the inclusion of BLN does not lead to a change in model performance of $SO_2$ representation in the boundary layer. ECHAM significantly underpredicts the magnitude of $SO_2$ at each site compared to the observations and both UKESM variants. The observation results for Pallas are consistent with Jordan et al. (2024), they did not include $SO_2$ for Zeppelin during September as they required consistent coverage with $SO_4$ data.

https://doi.org/10.5194/egusphere-2026-1043
Preprint. Discussion started: 11 May 2026


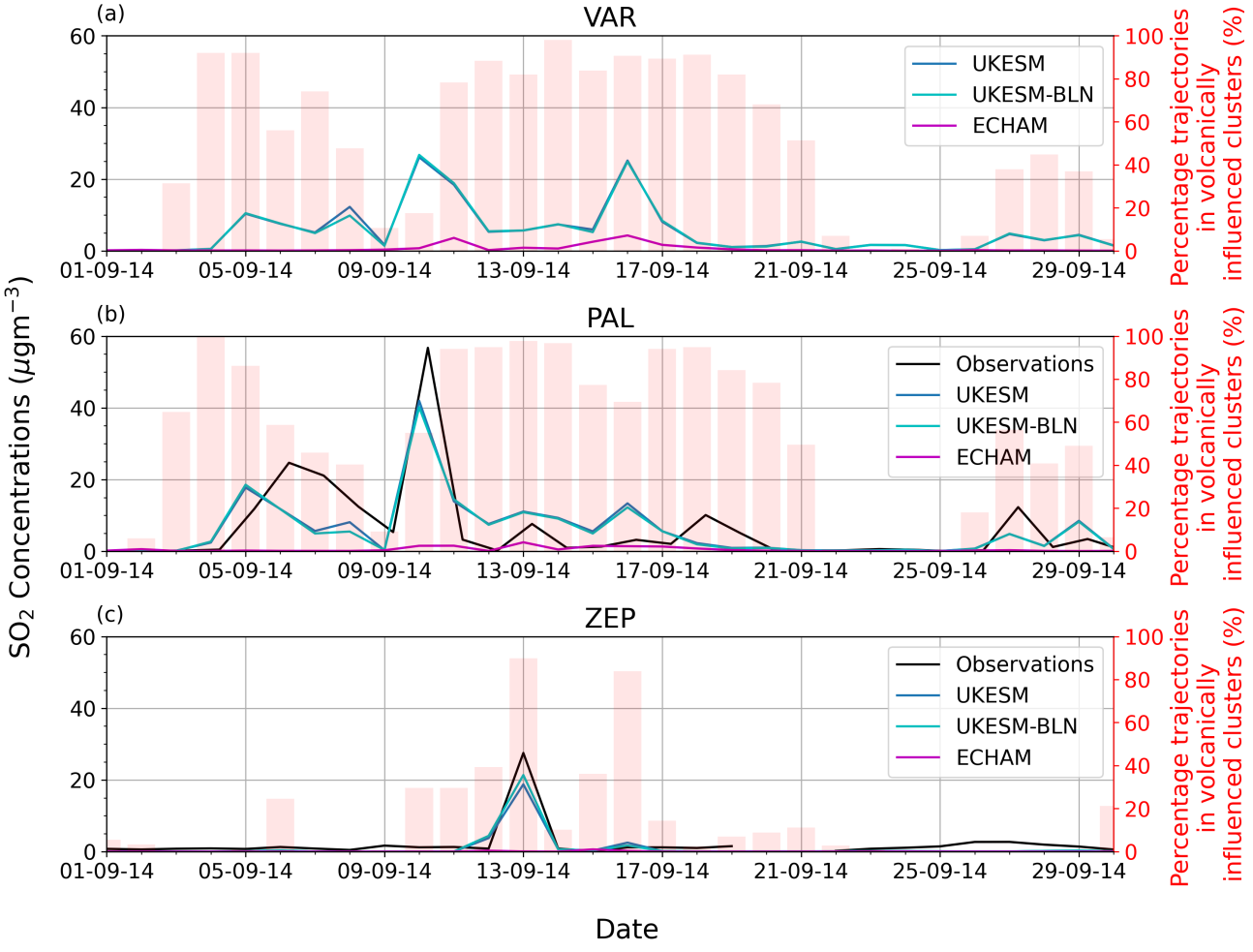


**Figure 5: Timeseries of $SO_2$ concentrations during September 2014 at each site in-situ measurement site: (a) Värriö, (b) Pallas and (c) Zeppelin. Observations are shown in black, UKESM1.0 in blue, UKESM1.0-BLN in cyan and ECHAM6.3-HAM2.3 in magenta. We note that observations of $SO_2$ were not available at Värriö during the eruption period. The red bars indicate the percentage of trajectories per day in the volcanically influenced clusters defined in section 2.7.**

### 3.2 Aerosol size distribution during eruption

To investigate the impact and the model representation of the eruption at the sites we next consider the aerosol size distribution timeseries at Värriö (Fig. 6). Värriö has the most consistent coverage for September 2014 (Fig. 6) compared to the other two sites (Figs. S3 and S5) and thus is used for as the focus for the analysis throughout.

https://doi.org/10.5194/egusphere-2026-1043
Preprint. Discussion started: 11 May 2026


Throughout the DMPS size distribution timeseries for September 2014 characteristic 'banana' curves (Kerminen and Kulmala, 2002) associated with NPF are observed (Fig. 6). The subsequent growth for some of these events are particularly long-lived compared to the standard duration for formation and sustained growth of an event at Värriö, found to be on average 17 hours from a machine learning NPF detection method (Su et al., 2022), or typically 6-24hrs considering the time span (from newly formed mode is observable until no longer distinguishable) at Värriö (Hussein et al., 2009). There is a persistent growth event from the 15$^{th}$ of September (Fig. 6a), which persists over several days with growth from less than 10nm to the accumulation size range around 250nm. The clear growth pattern after an NPF event is an indication that it occurs over a large spatial scale (Tunved et al., 2003), with the spatial scale linking to the time span of the event (Hussein et al., 2009). The newly formed particles have a chance to grow if the pre-existing aerosol particle number concentrations are low enough, resulting in low condensation and coagulation sinks (Dal Maso et al., 2007). Rare, sustained growth events spanning up to 5 days have been previously identified at in-situ boreal sites, for which it takes a long time before the newly formed aerosol particles are removed by incoming air masses because aerosol particles retain similar physical characteristics over a large spatial scale (Hussein et al., 2009). Other studies have found have similarly suggested homogenous NPF over a large area and have suggested key conditions for these phenomena are a low condensation sink, high availability of precursor gases and stable atmospheric conditions (Tröstl et al., 2016). In this case we have a consistent airmass associated with transport from the volcano, which will offer high availability of precursor gases, leading to homogenous NPF over a large area, thus facilitating the long-lived growth events seen in the time series of the size distribution (Fig. 6a).

https://doi.org/10.5194/egusphere-2026-1043
Preprint. Discussion started: 11 May 2026


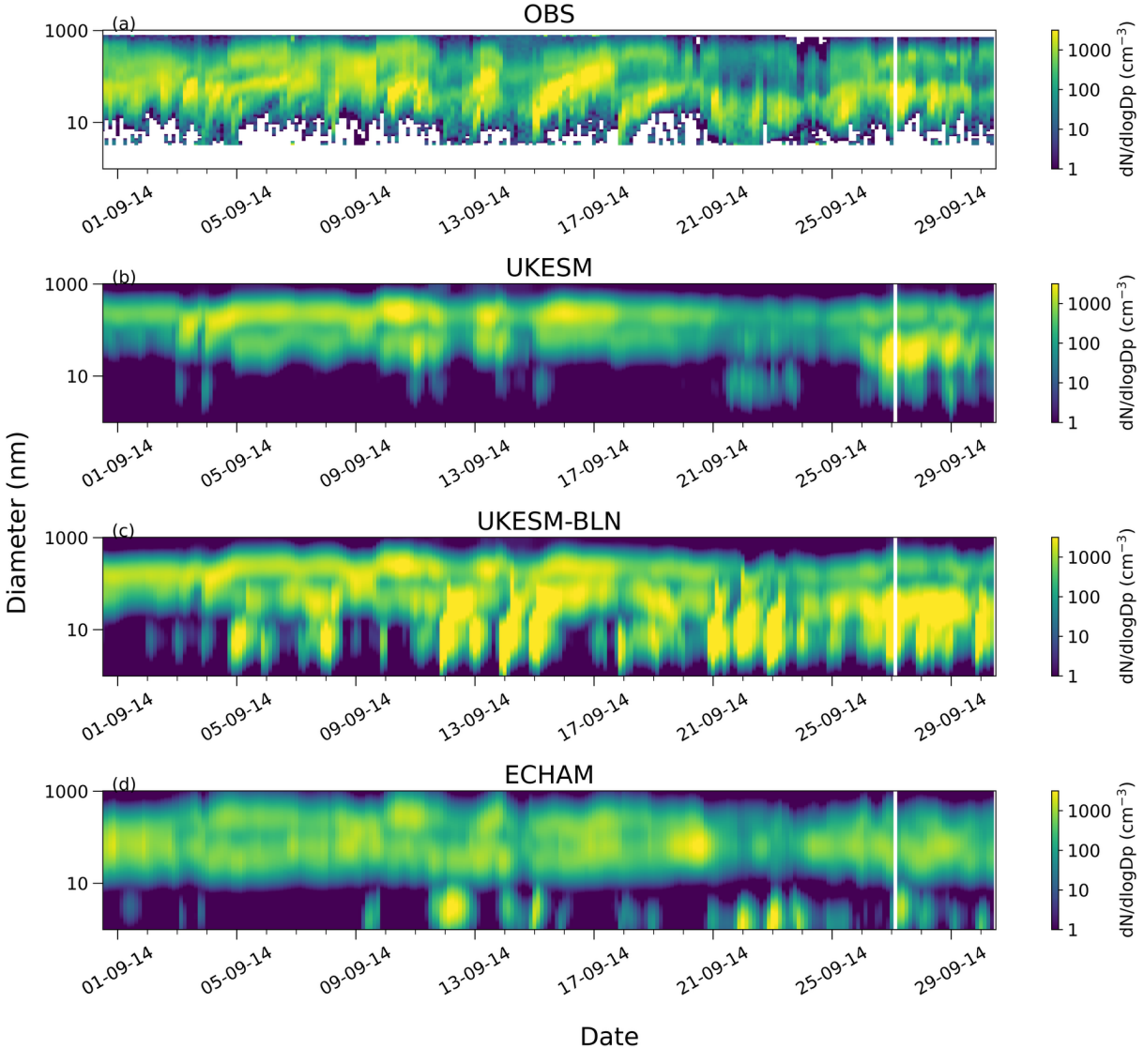


**Figure 6: Timeseries of size distribution for September 2014 at Värriö in dN/dlog$D_p$. (a) observations (DMPS), (b) UKESM1.0, (c) UKESM1.0-BLN and (d) ECHAM6.3HAM2.3. Note that the x axis labels and ticks indicate the date at midday.**

NPF events triggered by gas-phase conversion of $SO_2$ to $SO_4$ from Holuhraun have previously been identified for UK in-situ surface stations in a study by Twigg et al. (2016). NPF in a volcanic plume was first observed during the Eyjafjallajokull volcano eruption in Spring 2010 at the Puy de Dôme atmospheric research station in central France (Boulon et al., 2011), and it was found that NPF can occur within the lower troposphere at a large distance from the eruptive activity with an unusually high particle formation rate. Boulon et al. (2011) found that a binary $H_2SO_4$ - $H_2O$ nucleation scheme underestimated the observed particle formation rate by 7 to 8 orders of magnitude and suggested that it should not be applied in tropospheric

https://doi.org/10.5194/egusphere-2026-1043
Preprint. Discussion started: 11 May 2026


conditions. There remains little literature on the importance of NPF in volcanic plumes or the modelling of these processes, despite evidence of the importance of the mechanism for contribution to CCN (Boulon et al., 2011; Rose et al., 2019; Sahyoun et al., 2019). The impact of the addition of organic-mediated boundary layer nucleation is explored for UKESM1.0, which as standard only includes neutral binary homogenous nucleation throughout the troposphere. The timings of the observed NPF events are well replicated by UKESM-BLN, and there is evidence of sustained growth after the NPF events. However, despite the inclusion of the reduced boundary layer nucleation rate (Ranjithkumar et al., 2021), the concentrations associated with the NPF events in UKESM-BLN lead to total concentrations (for $D_p$=10-800nm) that are an average factor of 1.98 too high over September (Table S9). Some NPF events, for example the 12$^{th}$ of September and 22$^{nd}$ of September have NMBF of up to 10, demonstrating a very high bias for UKESM-BLN (Figs. 7a and 7c).

In general, UKESM and ECHAM underpredict total aerosol number concentrations (Fig. 7c) by average factors of 1.67 and 1.77 respectively (Table S9). UKESM substantially underpredicts the Aitken mode, with a maximum absolute NMBF of 37.2 (Fig. 7a), but on average overpredicts the accumulation mode (Fig. 7b). Introducing organic-mediated BLN in UKESM-BLN, results in more accurate representation of the Aitken mode concentrations (Fig. 7a), but increased overprediction of the accumulation mode concentrations (Fig. 7b), highlighting the contribution of the organic-mediated BLN to all lognormal aerosol modes in UKESM.

Aitken concentrations are best replicated by ECHAM (Figs. 7a) throughout the eruption period, however, whilst there is evidence of nucleation particles during the eruption period for ECHAM coinciding with the timing of NPF events in the observations, there is no continuous growth from the nucleation mode to larger modes (Fig. 6d), as observed (Fig. 6a). NPF events without subsequent growth have been observed frequently in previous studies and have been classified 'class II' (Dal Maso et al., 2005), 'apple' events (Manninen et al., 2010) or type 2 (e.g. Lee et al., 2020). This type of event, where there is a burst of particle formation but no subsequent growth, is often associated with a high condensation sink or too low concentrations of precursor gases in observational studies. Modelling studies have found similar lack of growth of aerosols from NPF events at boreal sites; however, this is often attributable to model artifacts. Svenhag et al. (2025) tested many different nucleation mechanisms in EC-Earth and found that the GCM was able to replicate the timing of events in the boreal forest, but not subsequent growth. A study investigating the treatment of BVOC-SOA in GCMs found that for ECHAM the phenomenon was a model artifact and suggested that it was associated with the size of particles added to the nucleation mode (Sporre et al., 2020). The size at which the particles are added is important for the transfer of particles into the Aitken mode, as the addition of newly formed particles to the nucleation mode decreases the median diameter of the mode and thus can decrease the number of particles transferred to the Aitken mode (Sporre et al., 2020), which could lead to the lack of growth into larger sizes. The representation of mode merging could also play a role in the lack of sustained growth from NPF events in ECHAM (Korhola et al., 2014).

https://doi.org/10.5194/egusphere-2026-1043
Preprint. Discussion started: 11 May 2026


Results are consistent for Pallas with sustained NPF events observed during the eruption period (Fig. S3a, 14-17$^{th}$ of September), for which the growth into larger sized particles are only represented by UKESM-BLN. ECHAM most accurately represents the magnitude of the Aitken mode concentrations (Fig. S4a) but demonstrates no growth from NPF events to larger sizes, as found for at Värriö. We note that Pallas has more missing PNSD data during the eruption period, reducing the statistics available to investigate the perturbation as well as Lagrangian analysis.

For Zeppelin we note that the peak of $SO_2$ concentration at Zeppelin (around the 13$^{th}$ of September) (Fig. 5c) coincides with missing data in the PNSD (Fig. S5), as well as much of the dates with transport associated with the volcano (Figs. S5 and S6), thus there is less data available for the analysis of the eruption at Zeppelin. There is no evidence of sustained NPF growth events at Zeppelin, contrasting to the boreal sites in the PNSD timeseries (Fig. S5). UKESM again underpredicts Aitken concentrations, however contrastingly, at Zeppelin UKESM-BLN also underpredicts Aitken mode concentrations. The Metzger BLN scheme has shown a general lack of nucleation in oceanic regions due to low concentration of organics required for the oxidation mechanism (Metzger et al., 2010) but was not developed or tested with data from the Arctic, and has been shown to underestimate nucleation and Aitken mode concentrations during the freeze period (after the end of August) (Price et al., 2023). ECHAM shows high concentrations of nucleation mode sized particles (Fig. S5d), but due to the instrument limit for the observations this cannot be evaluated. ECHAM best replicates the Aitken mode concentrations (Fig. S6a) but underpredicts accumulation mode concentrations more than both UKESM configurations (Fig. S6b). UKESM-BLN consistently has higher concentrations of accumulation mode particles, suggesting contribution of organic-mediated NPF in the boundary layer from further afield to the accumulation mode population, leading to improved skill overall (UKESM-BLN underpredicts the total aerosol number concentrations by a factor of 1.6 compared to 2.24 for UKESM, Table S9).

https://doi.org/10.5194/egusphere-2026-1043
Preprint. Discussion started: 11 May 2026


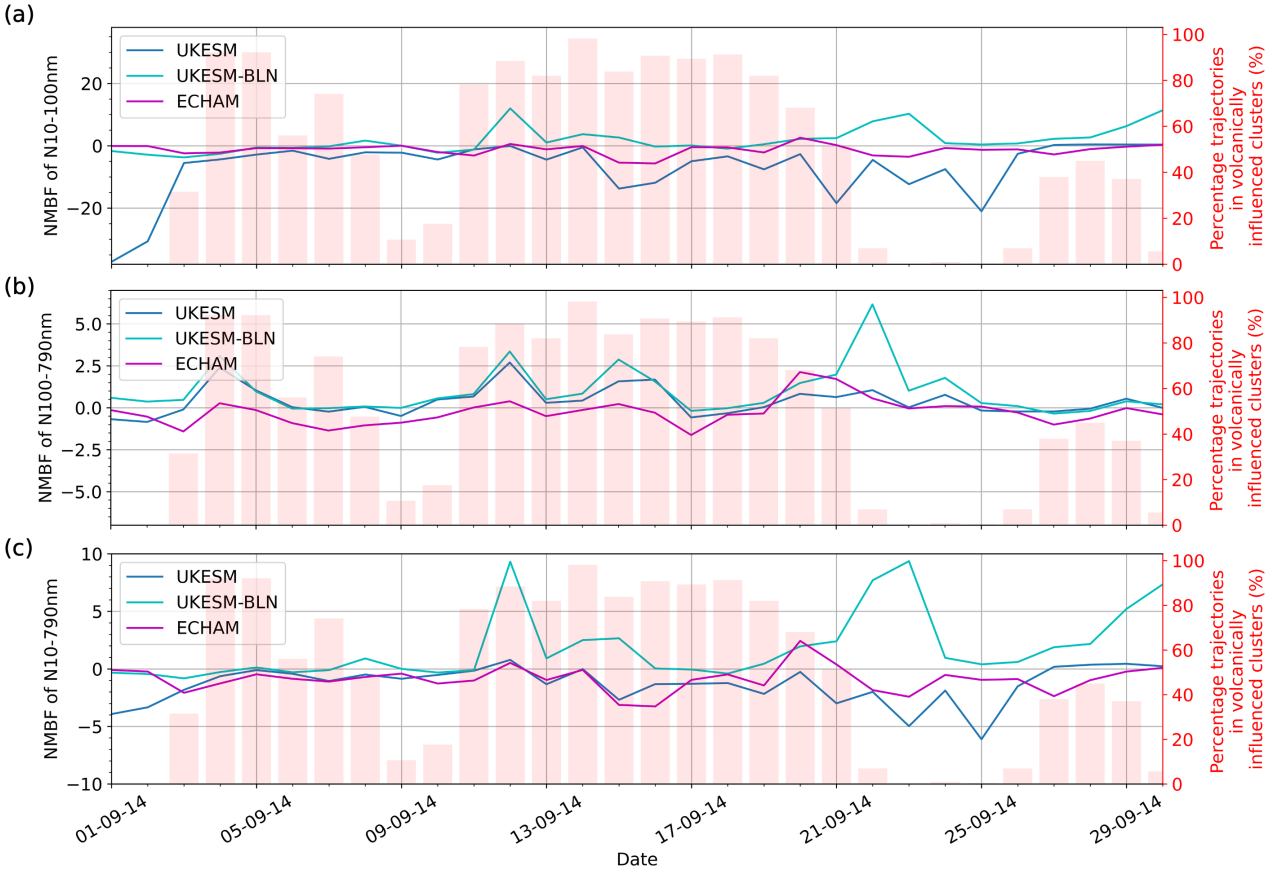


**Figure 7: Timeseries of normalised mean bias factor (NMBF) (Eq. 4) per day during September 2014 at Värriö for different size ranges for each model compared to observations: (a) Aitken mode (10-100nm) (b) accumulation mode (100-790nm) and (c) total (10-790nm). UKESM1.0 is shown in blue, UKESM1.0-BLN in cyan and ECHAM6.3-HAM2.3 in magenta. The period which was found to be influenced by transport from the volcano from the clustering analysis (Sect. 2.7) is indicated by the red shading of the timeseries.**

Under standard conditions, NPF events are frequently observed at Boreal and Arctic measurement sites and have been found to contribute to the formation of CCN sized particles (Beck et al., 2021; Spracklen et al., 2008; Tunved et al., 2006), thus are key to ensure accurate representation of ACI in GCMs. Here for the first time, we have compared UKESM configurations and ECHAM representation of NPF events during the Holuhraun eruption through 3-hourly PNSD analysis, highlighting the ability of UKESM-BLN to capture the timing of events and some growth into the CCN size range. In the next phase of analysis, the average size distribution is compared to a climatology (September 2009-2013), to further investigate the impact of the eruption on the physical properties of the aerosol particle number size distribution at the in-situ sites.

https://doi.org/10.5194/egusphere-2026-1043
Preprint. Discussion started: 11 May 2026


### 3.3 Perturbation of aerosol size distribution compared to climatology

The average size distributions from the clusters associated with transport from the eruption region were compared between the eruption period (September 2014) and a climatology (September 2009-2013 for Pallas and Värriö, and 2010-2013 for Zeppelin) for each measurement site (Fig. 8). The average size distributions are spatially filtered, using the clusters identified in Sect. 2.7, to remove potential of anthropogenic influence for both the climatology and eruption period averages, focusing on transport from Iceland over the North Atlantic. The average size distributions for the full time-period, without filtering transport pathways, are shown in the supplementary material (Fig. S7), where the volcanic perturbation is still evident. We note that all the GCMs in this study use modal schemes with fixed geometric size distribution (GSD), thus there will be no changes to the width of the modes. Analysis instead focuses on the changes in number concentration and average modal diameters.

Typically, September at the Finnish sites, particularly Värriö, has been found to be associated with a weak secondary peak in NPF after a maximum in the springtime (Asmi et al., 2011; Dal Maso et al., 2008; Komppula et al., 2006; Kyrö et al., 2014), and on average total, Aitken mode and accumulation mode number concentrations are decreasing in September after a summer peak (Dal Maso et al., 2008). At Zeppelin aerosol mass and number concentrations are typically at a minimum during September/ October (Croft et al., 2016; Tunved et al., 2013), and in September the frequency of NPF starts to decrease after a summer peak in Arctic, with type 2 events contributing a greater role (Lee et al., 2020), likely associated lack of gas phase precursors (Dall'Osto et al., 2017).

During the eruption in September 2014 there is a distinct trend across all three sites in the observations: an increase in the modal diameter for the accumulation mode compared to the climatology (Fig. 8a-c). The increase in modal diameter of particles is further highlighted when considering the surface area of particles (dS/dlogDp) (Fig. S8) which would correspond to an increase in the condensation sink. Pallas demonstrates a decrease in the Aitken mode diameter (Fig. 8b) which is not evident at Värriö, perhaps due to the comparative proximity to the eruption and the time for growth during transport between the sites (Väänänen et al., 2013).

We note that Zeppelin additionally demonstrates a substantial decrease in Aitken mode concentrations during the eruption (Fig. 8c), which is not evident at the Boreal sites, which could suggest suppression of NPF and increased coagulation and condensation from the volcanic perturbation leading to the decreased concentrations, but increased modal diameters for the Aitken and accumulation modes.

The GCM simulations exhibit very different responses to the perturbation in 2014 (Fig. 8). UKESM does not replicate the increase in accumulation mode diameter. It instead shows a significant increase in number concentration across the whole size distribution for Värriö and Pallas (Figs. 8d-e), but a smaller magnitude response at Zeppelin (Fig. 8f). ECHAM shows an increase in the diameter of all size modes at all three sites (Figs. 8j-l). UKESM-BLN is most representative of the observed

https://doi.org/10.5194/egusphere-2026-1043
Preprint. Discussion started: 11 May 2026


perturbation, demonstrating an increase in the accumulation mode diameter at all three sites (Figs. 8g-i). The differences in the representation of the perturbation suggests distinct processes controlling the aerosol response to the volcanic perturbation in the observations and GCMs, which will subsequently be explored. We note that the climatology of the average aerosol size distribution is not well represented by any GCM (Fig. 8), which will further perpetuate discrepancies in cloud properties with the large perturbation from Holuhraun, as the response of clouds to aerosols is non-linear (Carslaw et al., 2013) and strongly dependant on the aerosol baseline, as found in Marelle et al. (2025).

https://doi.org/10.5194/egusphere-2026-1043
Preprint. Discussion started: 11 May 2026


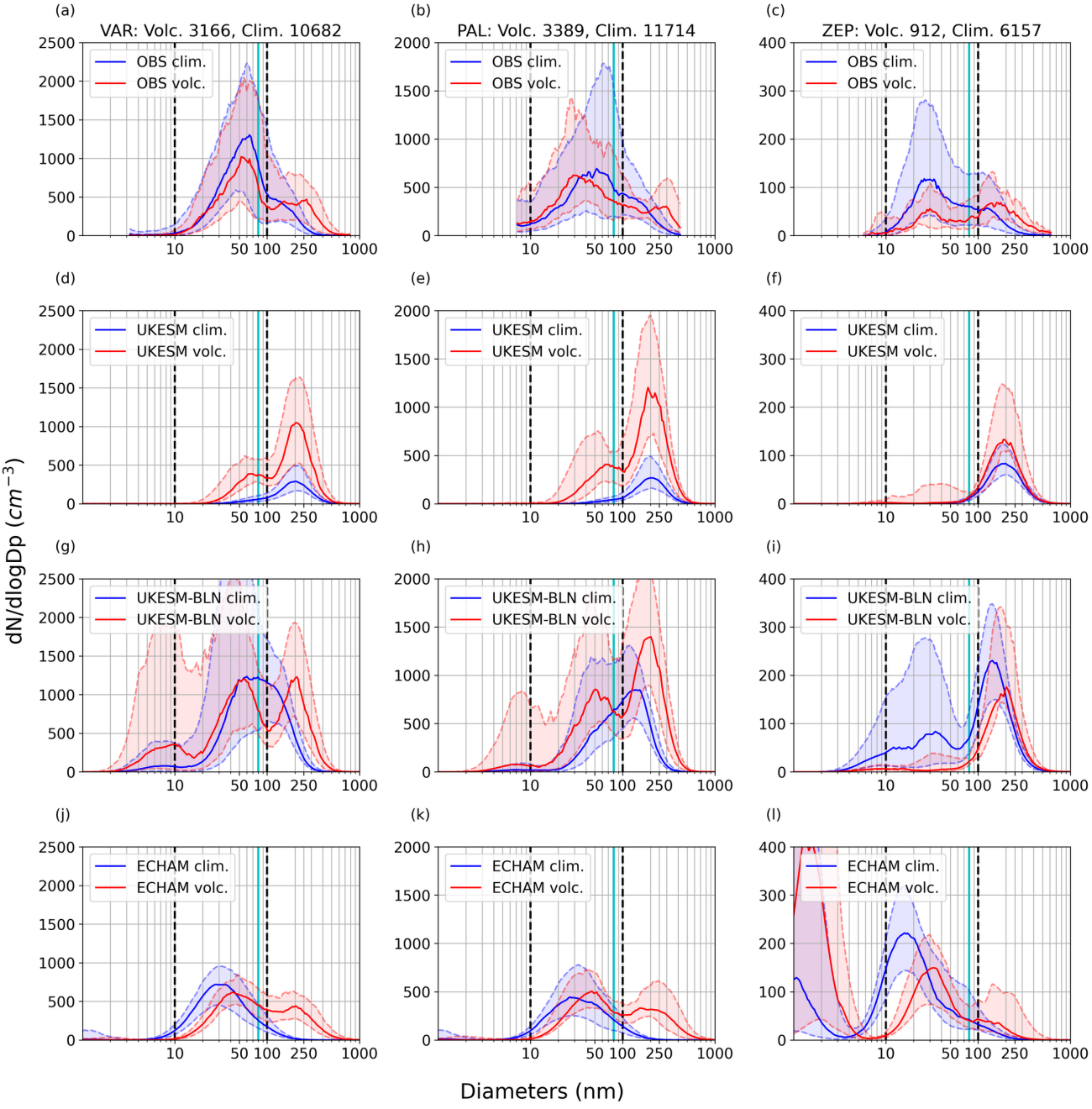


**Figure 8: Average size distribution for September at each site. (a-c) Shows observations (DMPS), (d-f) UKESM1.0, (g-i) UKESM1.0-BLN and (j-l) ECHAM6.3-HAM2.3. Red represents the eruption year (2014) and blue the climatology years (Värriö and Pallas: 2009-2013, Zeppelin: 2010-2013). Median indicated by solid line and 25th-75th percentiles by the shaded region. The size distributions are averaged based on data arriving from the direction of Holuhraun, based on the selected clusters in Sect. 2.7. The number of trajectories included in each average is indicated in the title of each column for the climatology and eruption period. The black dotted vertical lines indicate the separation of modes in this study: 1-10nm to represent the nucleation mode, 10-100nm to represent the Aitken mode and 100-800nm to represent the accumulation mode. The cyan vertical lines indicate the 80nm threshold used as a proxy for CCN in this study. Note that the y-axis limits are not consistent between sites.**

https://doi.org/10.5194/egusphere-2026-1043
Preprint. Discussion started: 11 May 2026


ECHAM replicates the observed size distributions well during the eruption period, but overestimates the Aitken mode concentrations for Zeppelin. However, during the climatology period, the mean diameter of the Aitken mode and the number concentrations for the accumulation mode are significantly underestimated. There is not a distinct accumulation mode, separated from the Aitken mode by the Hoppel minimum, as in the observations. Therefore, despite reasonable representation of the size distribution for the eruption year, as the baseline is not well replicated, this could result in a substantial difference in the radiative forcing associated with the eruption at the sites compared to observations. The growth in accumulation mode diameter and lack of increase in particle number is suggestive of growth processes such as condensation, coagulation and cloud processing (Figs. 8j and 8k). In ECHAM there is complete removal of sulfuric acid gas in clouds and no aerosol nucleation takes place (Kazil et al., 2010; Zhang et al., 2012). Thus, in-cloud oxidation results in a population of particles with larger mass but not an increase in particle number. Contrastingly, the representation of the aerosol size distribution in ECHAM at Zeppelin shows a significant increase in the concentration of nucleation mode particles, suggesting a significant contribution of gas-phase oxidation (Fig. 8l).

In UKESM, the response of increased number rather than increased modal diameter for both Aitken and accumulation modes suggests gas-phase rather than aqueous-phase oxidation dominates. In UKESM, sulphate produced from aqueous-phase reactions is used to update the mass of soluble accumulation and coarse modes (Mulcahy et al., 2020), increasing mass and modal diameters but not increasing particle number (Turnock et al., 2019).

With the introduction of boundary layer nucleation for UKESM-BLN (Figs. 8g-i), there is a significant change in the representation of the perturbation to the aerosol size distribution. During the eruption there is an increase in the accumulation mode diameter, but no longer a consistent increase in the concentration of accumulation mode particles across the sites. There is an increase in the number of nucleation mode particles during the eruption at the Boreal sites, an increase of the accumulation mode diameter and deepening of the Hoppel minimum. We hypothesise that the growth processes such as coagulation and condensation of new particles formed through enhanced BLN during the eruption, with enhanced precursor gases, onto pre-existing particles, is resulting in the growth of the particles to larger diameters. At Zeppelin the response is different: there is a decrease in concentrations for all modes, but an increase at all modal diameters (Fig. 8i). The decrease in Aitken mode concentrations during the eruption is consistent with the observational dataset, however, the change in Aitken mode concentrations is more significant in UKESM-BLN than is observed. This suggests the coagulation and growth from the volcanic perturbation leading to an increase in the average Aitken and accumulation mode diameters, and a decrease in particle number concentrations in the Aitken and nucleation modes.

To understand the role of NPF on the CCN concentrations resulting from the Holuhraun eruption and the GCM ability to replicate the changes in size distribution, it is essential to understand the availability of precursor gases during transport as well as the condensation sink (Kulmala et al., 2001), which warrants a Lagrangian evaluation of these quantities.

https://doi.org/10.5194/egusphere-2026-1043
Preprint. Discussion started: 11 May 2026


## 4 Lagrangian GCM evaluation

To probe the differences in model representation that result in the inaccurate representation of the perturbation from the eruption, we conducted a GCM Lagrangian analysis which enables investigation of the processes during transport, focusing on Värriö as this site had the most coverage during the eruption period. 3-hourly resolution Lagrangian analysis provides a much tighter observational constraint than Eulerian analysis, as receptor models encapsulate both spatial and temporal information, which allows for more rigorous evaluation, ensuring the representation is due to the correct underlying mechanisms and not due to compensating errors.

### 4.1 Transport

To investigate the difference in the aerosol response we employ a Lagrangian evaluation, utilising reanalysis and GCM meteorology driven trajectories. Firstly, we evaluate the consistency in transport pathways between modelled and reanalysis trajectories during the eruption period.

The transport frequency receptor models (Fig. 9) are consistent between ERA-Interim, UKESM, UKESM-BLN and ECHAM. Which confirms that the nudging of the horizontal winds in the simulations produces consistent transport in the horizontal and that the differences in $SO_2$ concentrations and aerosol size distributions are not associated with differences in transport. There are some differences in the average altitude of trajectories during transport, which is not unexpected and could be due to several factors: the nudging only being applied to the horizontal winds, a relaxation time of 6 hours, the difference in the application of the nudging between models, and the resolution. However, for the region of focus for the influence of the Holuhraun eruption, over the North Atlantic, transport from Iceland is consistently low (Fig. 9).

https://doi.org/10.5194/egusphere-2026-1043
Preprint. Discussion started: 11 May 2026


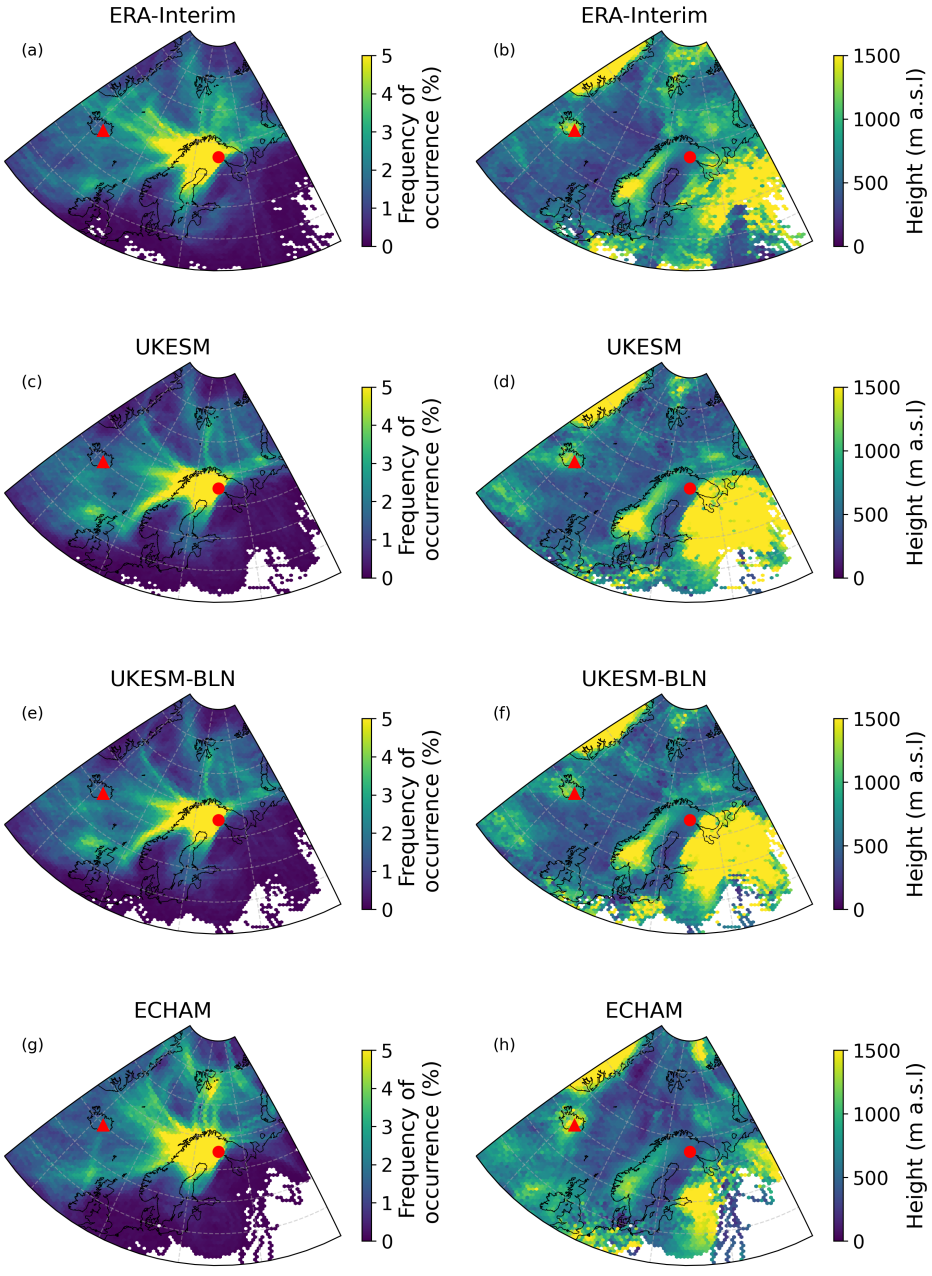


545 **Figure 9: The transport frequency receptor models (a, c, e and g) (Eq. 1) as well as the average height (a.s.l.) (b, d, f and h) for back trajectories passing through a grid cell, calculated using the CVT receptor model (Eq. 3). For all trajectories initialised at Värriö during September 2014, for ERA-Interim (a-b), UKESM1.0 (c-d), UKESM1.0-BLN (e-f) and ECHAM6.3-HAM2.3 (g-h).**

https://doi.org/10.5194/egusphere-2026-1043
Preprint. Discussion started: 11 May 2026


### 4.2 $SO_2$ to $SO_4$ conversion

Collocating the GCM 3-hourly $SO_2$ gas and $SO_4$ aerosol fields onto the GCM trajectories enables investigation of the spatial and temporal evolution of these variables within the plume during transport for the GCMs, utilising the CVT framework (Eq. 3), to isolate the differences that could lead to differences in the aerosol perturbation. Similarly, from the $SO_2$ and $SO_4$ fields, the total sulphur (S) is estimated and evaluated in the CVT framework. UKESM and UKESM-BLN are consistent in the mass concentrations of S and the conversion of $SO_2$ to $SO_4$ (Fig. 10a-h). However, there is a clear discrepancy for ECHAM: the plume of S does not extend as far into the North Atlantic compared to UKESM (Figs. 10a, and 10i). The difference is highlighted further when considering the separate components of S (Figs. 10j and 10k). For $SO_2$ there are only high $SO_2$ concentrations in the vicinity of the vent in ECHAM (Fig. 10j), whereas there is a plume of high concentrations of $SO_4$, from the eruption site, across the North Atlantic (Fig. 10k), compared to the higher concentrations of $SO_2$ in the North Atlantic in UKESM (Fig. 10b) and lower concentrations of $SO_4$ (Fig. 10c). Concentrations of $SO_4$ at the measurement sites are more consistent in magnitude between both UKESM versions and ECHAM (Figs. 10c, 10g and 10k). However, the conversion clearly occurs much earlier during transport and therefore close to the vent in ECHAM.

Jordan et al. (2024) used an exponential decay relationship to derive the near-vent $SO_2$-$SO_4$ ratio of $25 \pm 5$ using a network of in-situ measurement sites, which agreed with the ratio derived in Ilyinskaya et al., (2017). Boichu et al. (2019) estimated a slightly lower ratio of 19.7 using a linear model. Using the CVT receptor model, the UKESM variants reveal $SO_2$-$SO_4$ ratios in the plume over the North Atlantic between ~10-40, with higher values around the vent (approximately 60) (Figs. 10d and 10h). We find that ECHAM demonstrates considerably lower ratios across the region considered, with a near vent ratio (of approximately 5) 4-6 times lower than any of these observationally derived estimations (Fig. 10l), which is consistent with the underestimation of $SO_2$ at the measurement sites (Fig. 5). Similarly in Jordan et al. (2024), ECHAM6.3-HAM2.3 was found to have the lowest near-vent $SO_2$-$SO_4$ ratio compared to the four other GCMs and chemical transport model (CTM), whereas UKESM1.0 had one of the most comparable $SO_2$-to-$SO_4$ ratios to those observed. The Lagrangian analysis undertaken here suggests that this is due to the overly efficient conversion of $SO_2$-to-$SO_4$ near the vent in ECHAM.

https://doi.org/10.5194/egusphere-2026-1043
Preprint. Discussion started: 11 May 2026


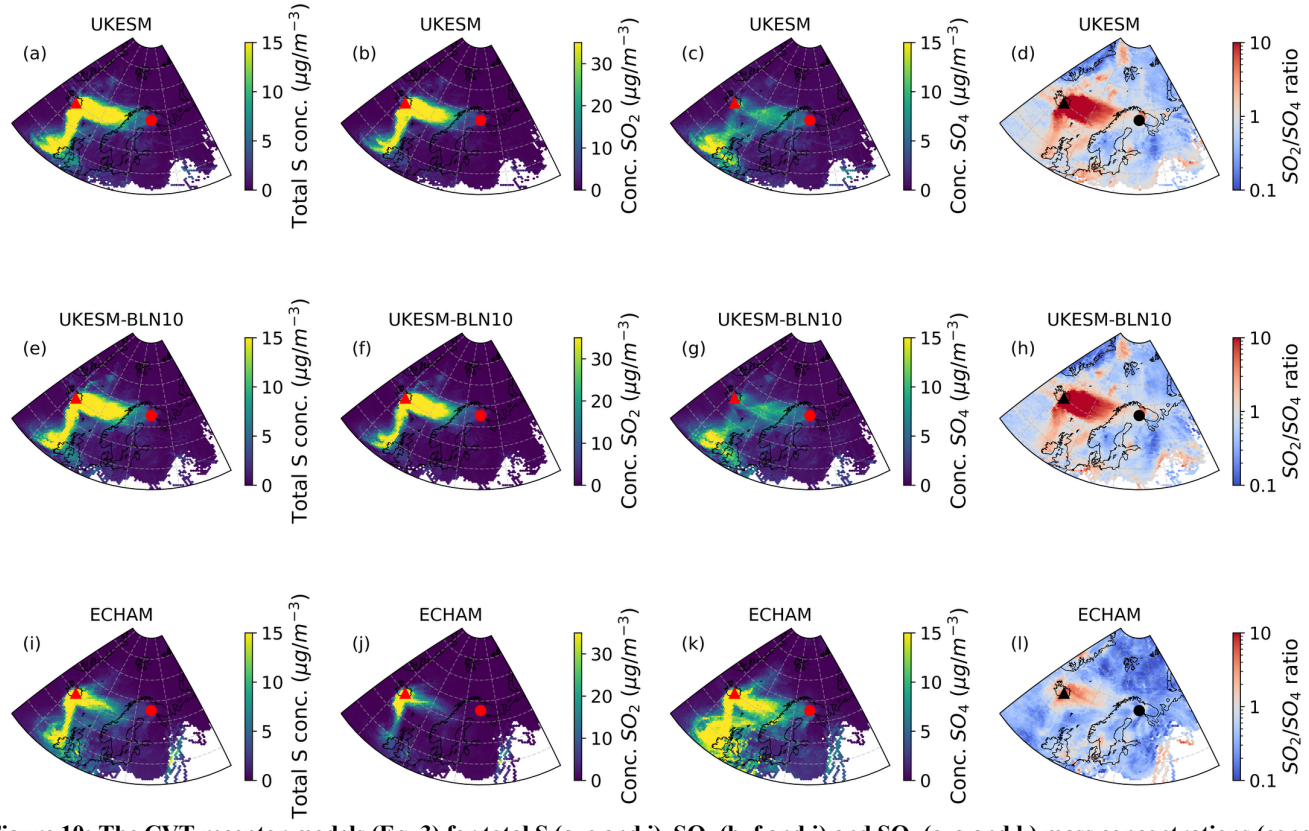


**Figure 10: The CVT receptor models (Eq. 3) for total S (a, e and i), $SO_2$ (b, f and j) and $SO_4$ (c, g and k) mass concentrations (conc.) collocated along back trajectories from Värriö. As well as the ratio of $SO_2$ to $SO_4$ (d, h and l). For UKESM1.0 (a-d), UKESM1.0-BLN10 (e-h) and ECHAM6.3-HAM2.3 (i-l).**

ECHAM atmospheric oxidants are prescribed by an 8-year climatology (Inness et al., 2013), whereas for UKESM the oxidants are interactively simulated and depleted by oxidation reactions (Sellar et al., 2019). This could lead to the differences in the conversion rate between ECHAM and UKESM, because in UKESM oxidation is limited by the available oxidants. The very high emission rates from the eruption are likely to exacerbate the impacts of oxidant limitation. Previous studies have highlighted the significant impact oxidant concentrations have on the total indirect effect, with lower oxidative power in the pre-industrial atmosphere extending the lifetime of precursor gases (Karset et al., 2018).

Cloud pH has been found to be an important factor in determining in-cloud oxidation rates as the preferential pathway for pH>5.5 is oxidation by ozone, which is highly sensitive to pH, whereas the preferential pathway for pH<5.5 is oxidation by hydrogen peroxide (Seinfeld and Pandis, 2006). Increasing pH by one unit can increase the oxidation rate by ozone by a factor of 100 (Kreidenweis et al., 2003). It has been long suggested that underestimation of in-cloud sulphate formation may contribute to the overestimation of $SO_2$ concentration and underestimation of sulphate mass particularly across polluted regions (Textor et al., 2006). Prior studies have noted the over prediction of $SO_2$ and underprediction of surface $SO_4$ in polluted

https://doi.org/10.5194/egusphere-2026-1043
Preprint. Discussion started: 11 May 2026


environments for UKESM1.0 (Hardacre et al., 2021), which could be associated with an underestimation of in-cloud sulphate formation.

We hypothesise that cloud pH is likely to be a significant contributing factor to the difference in oxidation rates between ECHAM and UKESM, as cloud pH is interactive in ECHAM (Tegen et al., 2019) and fixed at 5 for UKESM (Mulcahy et al., 2020). Treatment of cloud pH in models has been shown to have large ramifications, altering aerosol size distribution and thus CCN concentrations and aerosol radiative effects (e.g. Kreidenweis et al., 2003; Roelofs et al., 2006). With a global composition climate model, demonstrating that for an increase in pH from 5.0 to 6.0 between 1970-2009, the all-sky aerosol radiative effect over the North Atlantic strengthened to -5.2$Wm^{-2}$ from -1.2$Wm^{-2}$ (Turnock et al., 2019).

As well as the timing of oxidation during transport, there are many factors which are key in determining the aerosol populations resulting from the oxidation of $SO_2$ including the existing aerosol baseline, e.g. the condensation sink, which is discussed in the subsequent section.

### 4.3 Mechanisms controlling growth

To investigate the potential role of NPF in the perturbation of aerosol size distribution associated with the volcano, analysis of the condensation sink, available precursors ($SO_4$) and the nucleation mode ($D_p$=1-10nm) concentrations in the models during transport to the measurement site were conducted utilising the CVT receptor model (Fig. 11).

The condensation sink distribution in the CVT framework is generally consistent across the three models (Figs. 11a, 11d and 11g). However, in the plume, ECHAM demonstrates a lower condensation sink (Fig. 11g). Despite the condensation sink being high in the vicinity of the vent, $SO_4$ levels are high enough to sustain nucleation in UKESM and UKESM-BLN. In ECHAM, despite higher concentrations of $SO_4$ and a lower condensation sink in the plume, there is no nucleation in the plume (Figs. 11g-i). However, there are high concentrations of nucleation mode particles at the eruption site, suggesting condensation and coagulation or growth due to in-cloud oxidation during transport in ECHAM (Fig. 11i). Nucleation mode (1-10 nm) concentrations are very low in UKESM compared to the other GCMs (Figs. 10c, 10f and 10i), with concentrations only found in the region of the North Atlantic closest to the vent. This is consistent with previous studies that have suggested that the binary $H_2SO_4$-$H_2O$ nucleation scheme is not able to replicate the unusually high formation rate of NPF in volcanic plumes (Boulon et al., 2011). In UKESM-BLN there are high concentrations of nucleation particles close to the vent (Fig. 11f), much higher than those associated with the binary neutral homogeneous $H_2SO_4$-$H_2O$ nucleation in UKESM (Fig. 11c).

Interestingly, the distribution of nucleation particles not associated with the eruption is very distinct in UKESM-BLN (Fig. 11f) compared to ECHAM (Fig. 11i). High concentrations of nucleation mode particles are associated with transport over Europe and the UK for UKESM-BLN, likely associated with anthropogenic emissions (e.g. Alam et al., 2003; Bousiotis et al., 2021) in combination with organic mediated BLN over these forested regions. However, in ECHAM nucleation mode particles

https://doi.org/10.5194/egusphere-2026-1043
Preprint. Discussion started: 11 May 2026


are associated with transport over the Arctic, likely associated with charged nucleation of sulphuric acid and water which has been found to contribute most significantly (up to 70%) to concentrations of ultrafine aerosol in the BL over high latitude oceans due to cold temperatures and high ionisation rates in these regions (Kazil et al., 2010). These distinct nucleation source regions will result in different aerosol base states for the Holuhraun perturbation, particularly due to the difference in distance of nucleation particle formation from the measurement site, and thus the time for evolution and growth.

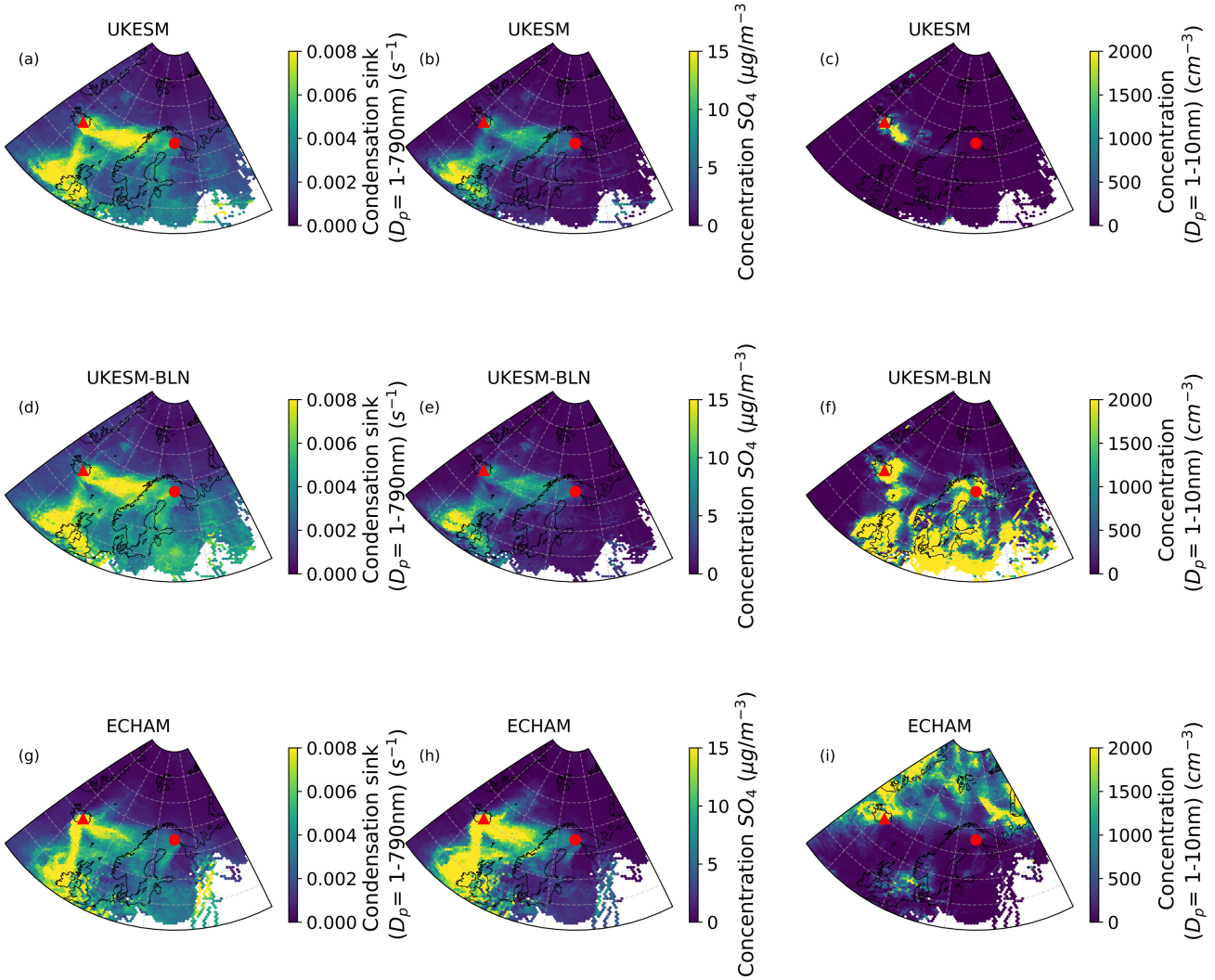


**Figure 11**: **The mean per grid cell of condensation sink (a, d and g), $SO_4$ mass concentrations (b, e and h) and nucleation mode (1-10nm) concentrations (c. f and i) collocated along back trajectories from Värriö, i.e. collocated trajectory receptor model (CVT) (Eq. 3). For UKESM1.0 (a-c), UKESM1.0-BLN10 (d-f) and ECHAM6.3-HAM2.3 (g-i)**

https://doi.org/10.5194/egusphere-2026-1043
Preprint. Discussion started: 11 May 2026


### 4.4 Differences in the spatial distribution of modal concentrations

Utilising the CWT framework (Eq. 2), we investigate the mechanisms that control the differences in the aerosol particle size distribution in comparison to the observations, utilising CWT receptor models of the modal concentrations, which highlight potential source regions. Unfortunately, due to the measurement limits of the instrument (DMPS) we cannot validate against observed nucleation mode concentrations.

First considering observations combined with ERA-Interim trajectories (Figs. 12a-d). Airmasses originating from the clean regions of North Atlantic and Arctic are associated with NPF at Boreal in-situ measurement sites (Dal Maso et al., 2007; Sogacheva et al., 2005). As discussed in Sect. 2.2 we cannot evaluate against observations for the nucleation mode concentrations. We instead investigate the observational Aitken mode particle concentrations, which show evidence of high concentrations associated with transport from these typically clean regions (Fig. 12b), which could be associated with growth of particles formed in NPF events. High accumulation mode concentrations are associated with transport from the volcano, with a defined plume evident in the CWT receptor framework (Fig. 12c), as well as high concentrations associated with transport from Eastern Europe and Russia (Fig. 12c).

We must note the ability of the models to successfully replicate the spatial distribution of the plume in the accumulation mode with variations in the representation of the magnitude (Figs. 12c, 12g, 12k and 12o). Thus, using this novel framework we can transparently reveal that the GCMs can reproduce increased concentrations of accumulation mode particles at the ground-based measurement site associated with transport from the eruption site.

Considering the representation of other aerosol modes, allows us to explore the GCM representation of the aerosol lifecycle during transport. UKESM demonstrates consistently low nucleation mode concentrations associated with transport from all directions, all of which will be associated with transport over the boreal forest. Thus, low nucleation mode concentrations are likely due to the lack of an organic-mediated BLN parameterisation (Fig. 12e). UKESM replicates the location of potential source regions compared to the observations in the CWT receptor model for the Aitken mode (Fig. 12f) associated with transport from the Arctic and Baltic seas, and underestimates concentrations of Aitken mode concentrations associated with the plume (Fig. 12f). High accumulation mode concentrations are associated with transport from the region of the Holuhraun plume, Eastern Europe and the Baltic Sea (Fig. 12g). High nucleation mode concentrations at the Holuhraun site evident in the CVT receptor model (Fig. 11c), are not seen in the CWT framework (Fig. 12e). As CVT receptor models show the average evolution of the concentration during transport, this also incorporates the impact of vertical transport. Over Iceland in the average trajectory heights are around 1000m a.g.l (Fig. S9), which could suggest that there is transport from the free troposphere, where nucleation preferentially takes places in the Vehkamäki et al. (2002) scheme used in UKESM1.0. This could suggest why there is nucleation in the CVT maps for UKESM but not the CWT maps. Instead in the CWT receptor model the transport pathway in the plume is associated with high accumulation mode concentrations, suggesting that the

https://doi.org/10.5194/egusphere-2026-1043
Preprint. Discussion started: 11 May 2026


nucleation particles formed at the volcano site coagulate and grow into accumulation mode sizes during transport to the measurement site.

Contrastingly, UKESM-BLN demonstrates high concentrations associated with transport in the plume for all modes, highlighting the contribution of NPF at different stages of transport, not just at the vent. High concentrations of Aitken mode particles associated with transport from the Arctic and North Atlantic correlate with high concentrations of nucleation mode particles (Figs. 12i-12j), which are the regions associated with NPF at Boreal in-situ measurement sites (Dal Maso et al., 2005), however the magnitude is considerably overestimated compared to observations (Fig. 12c). Comparing the CWT receptor model to the CVT model for nucleation mode particles in UKESM-BLN, the distribution is substantially different (Figs. 12i and 11f). The high nucleation mode concentrations associated with transport from the Arctic and North Atlantic in the CWT model (Fig. 11f) are not replicated by the CVT model which instead shows high concentrations up to the coastline for transport from North and West (Fig. 12i). This highlights the difference between the two receptor models – the CWT framework demonstrates the measurements at the site are associated with this transport corridor, however the CVT model suggests that this is due to NPF in the forest around the site rather than transport from further afield. The CVT model also highlights high nucleation mode concentrations over Europe and the UK in UKESM-BLN (Fig. 11f), compared to the CWT model (Fig. 12i) for which these regions are associated with accumulation mode concentrations, which suggests the evolution of the aerosol during transport. For UKESM-BLN modal concentrations are consistently too high compared to observations, particularly for the Aitken mode (Fig. 12j). However, the condensation sink over Eastern Europe and Russia (Fig. 12l) is lower than the observations (Fig. 12d), suggesting an underprediction of the size of aerosol formed from the anthropogenic sources in these regions.

https://doi.org/10.5194/egusphere-2026-1043
Preprint. Discussion started: 11 May 2026


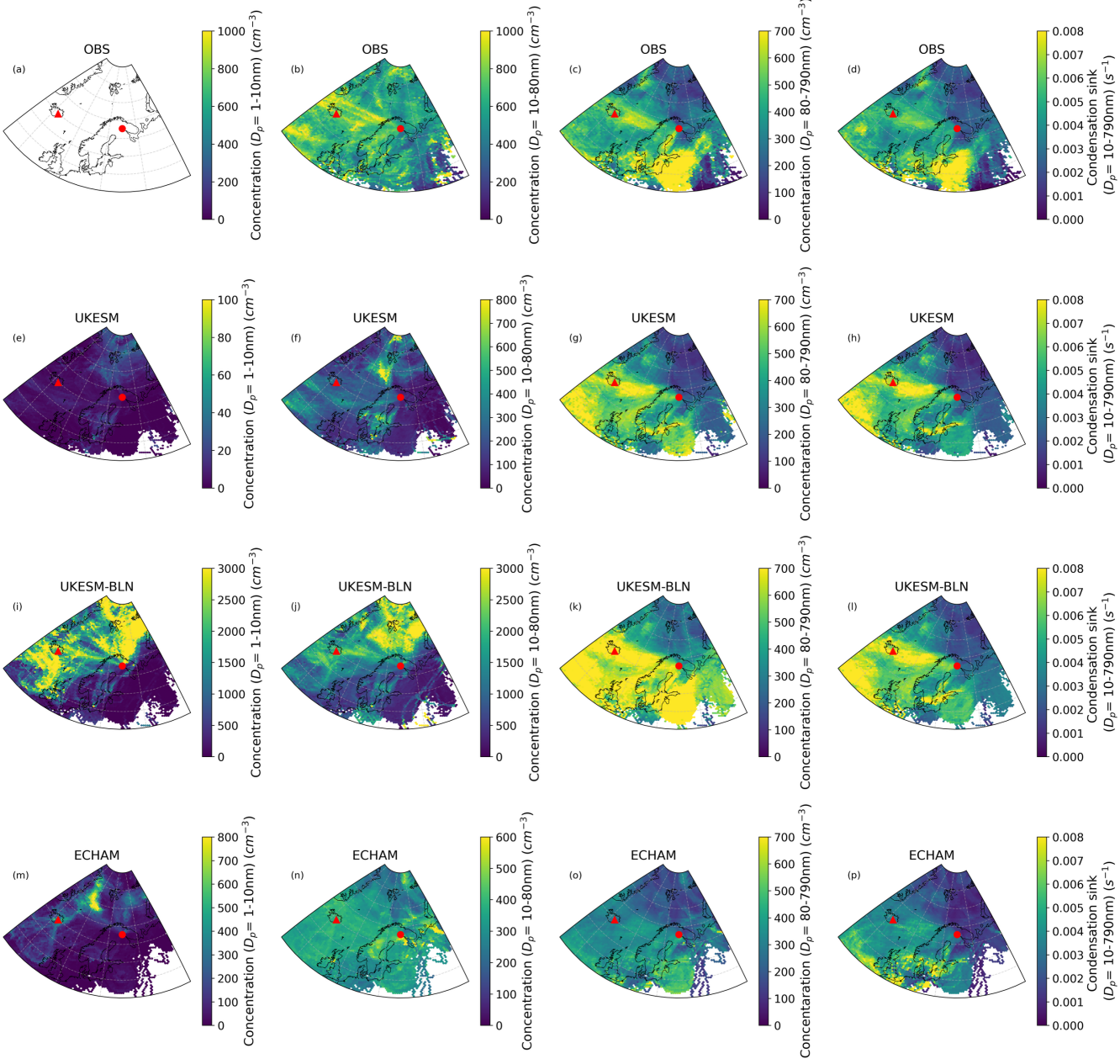


**Figure 12: The mean per grid cell of concentration of nucleation mode (1-10nm) (a, e, i and m), Aitken mode (10-100nm) (b, f, j and n) and accumulation mode (100-790nm) (c, g, k and o) particles and condensation sink (d, h, l and p) with back-trajectories starting from Värriö, using the CWT receptor model (Eq. 2). For observations with ERA-Interim trajectories (a-d), UKESM1.0 (e-h), UKESM1.0-BLN10 (i-l) and ECHAM6.3-HAM2.3 (m-p) during September 2014. Note that due to lack of consistent measurements for $D_p$=1-10nm the nucleation mode CWT is not included for the observations.**

https://doi.org/10.5194/egusphere-2026-1043
Preprint. Discussion started: 11 May 2026


### 4.5 Potential impact on cloud microphysics

After evaluating the impact on aerosol size distributions, we now consider the potential impacts that the differences found in the mechanisms and climatologies between GCMs and observations will have on the changes in CCN, which informs changes in cloud properties and radiative forcing.

We utilise the CWT framework with N80 (aerosol concentration for particles $D_p$>80nm) as a proxy for CCN (e.g. Asmi et al., 2011; Kerminen et al., 2012). This highlights the potential source regions of N80 and can be used to compare the differences between concentrations and potential sources between observations and GCMs (Fig. 13). To examine the sensitivity of N80 as a proxy for CCN, N100 was tested (Fig. S4). From this analysis we found consistent qualitative results between N80 and N100, in both the spatial distribution of potential source of CCN and the relative magnitudes between GCMs and observations. We note there are small changes in magnitude of concentrations as more bin diameters are included in the integration over the size distribution (Fig. S4).

Firstly, considering the climatology, highest concentration of N80 at the measurement site are associated with transport from Eastern Europe and Russia (Fig. 13). These regions are consistent across the observations and the three GCM simulations, however, the magnitude varies significantly (Figs. 13a, 13d, 13f and 13j), thus there is a difference in the baseline from which the models are representing the volcanic perturbation (Fig. S12), as previously found in the Eulerian framework (Sect. 3.3).

There are two key regions associated with large concentrations of N80 during the eruption period: eastern and central Europe and Russia, likely associated with anthropogenic pollution, and a clear North Atlantic plume from Iceland (Figs. 13b, 13e, 13h and 13k). The concentrations of N80 from the North Atlantic are significantly overestimated in UKESM, particularly in a region of high concentrations associated with transport south of Iceland, which is not present in the observations (Figs. 13b and 13e). In UKESM-BLN the spatial distribution is very consistent with UKESM, however the N80 concentrations are much higher (Figs. 13e and 13h). For ECHAM the concentrations of N80 are consistently lower over the region considered than for the observations (Figs. 13b and 13k). There is a 'plume' of high potential N80 concentrations in the same region over the North Atlantic compared to UKESM and the observations, but it is much less distinct (Fig. 13k).

Considering the difference between the climatology and eruption year (ΔN80) we see that all GCMs replicate an increase and demonstrate a clear plume associated with transport from the eruption site. There is generally an overestimation of the perturbation for CCN in UKESM (Fig. 13f) and ECHAM (Fig. 13l) compared to the observations (Fig. 13c). UKESM-BLN demonstrates the most consistent change in N80 in the CWT framework associated with the eruption for this study (Figs. 13i and 14b), as previously also found for the change in CDNC (Jordan et al., 2025). Considering the regression fit of the CWT frameworks for ΔN80 (Fig. 14), it is clear UKESM and ECHAM generally overestimate the change in N80, whereas UKESM-BLN demonstrates a much better fit to the observationally derived results (Fig. 14b), with a gradient of 0.8.

https://doi.org/10.5194/egusphere-2026-1043
Preprint. Discussion started: 11 May 2026


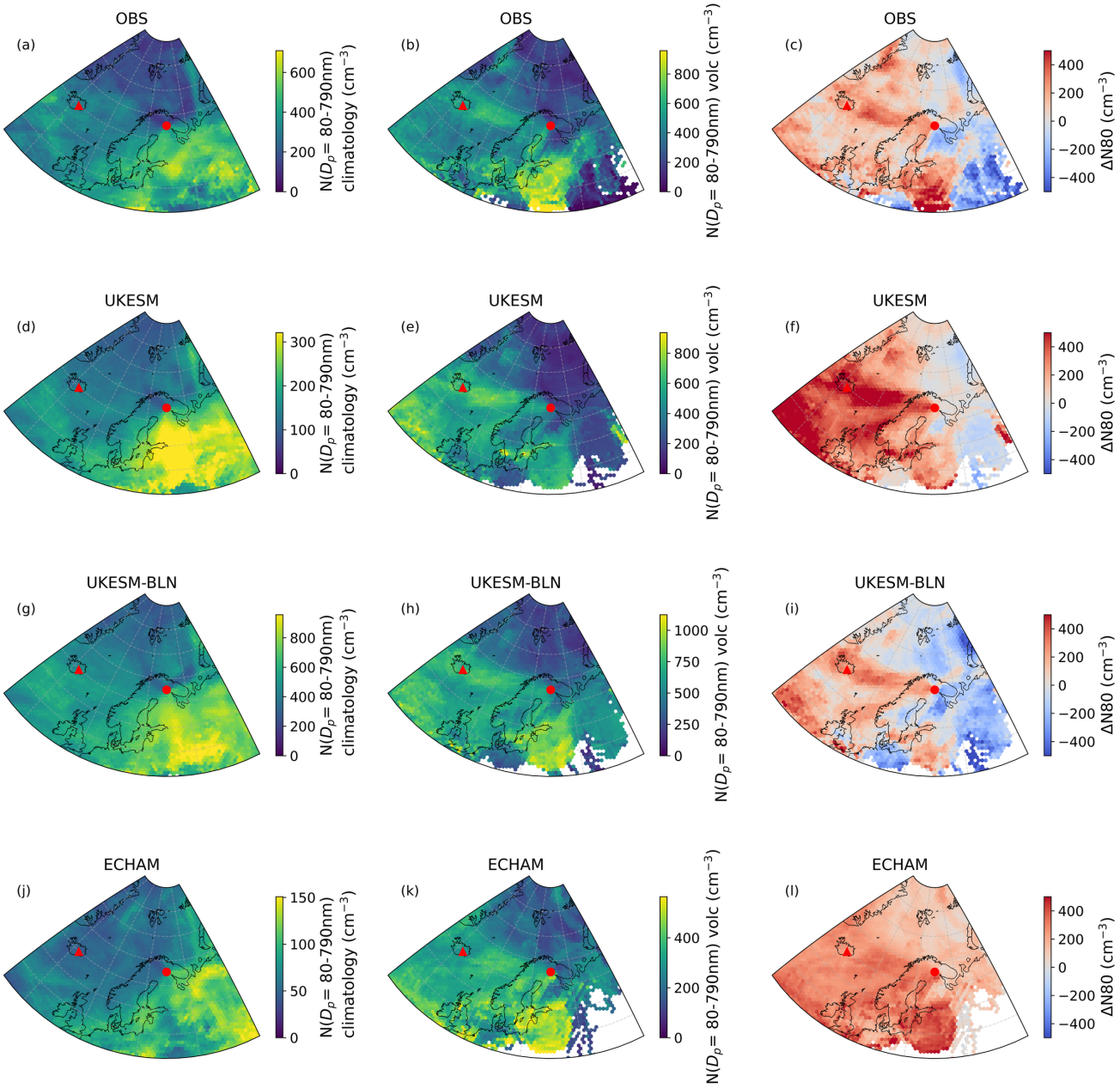


715 **Figure 13: The mean per grid cell for the concentration of particles above 80nm for the climatology (a, d, g and j), volcanic period (b, e, h and k) and the difference (volcanic period minus climatology) in concentration (c, f, i and l), utilising the concentration weighted trajectory (CWT) model (Eq. 2). For DMPS with ERA-Interim (a-c), UKESM1.0 (d-f), UKESM1.0-BLN10 (g-i) and ECHAM6.3-HAM2.3 (j-l). Note the difference in colour scale between subfigures.**

https://doi.org/10.5194/egusphere-2026-1043
Preprint. Discussion started: 11 May 2026


Comparing to the other sites, we find consistent results for Pallas in the spatial distribution of the plume (Fig. S11). However, we note that for Pallas the size limit to include in the CCN approximation, is much lower (430nm) compared to the other sites. UKESM-BLN best replicates the spatial distribution of the ΔN80 of the plume but overestimates the ΔN80 (Figs. S11c and S11i). At Zeppelin all GCMs demonstrate a clear plume in the CWT receptor models, however the magnitude of the ΔN80 plume is substantially overestimated compared to observations (Fig. S12). All models demonstrate distinct plumes of high N80 concentration and ΔN80 associated with the eruption (Fig. S12). In the observations the influence of the eruption plume on N80 is dwarfed by transport from Norway, Sweden, Finland and Russia (Fig. S12c), however in the ΔN80 the influence of the plume is clear over the North Atlantic. There is a decrease in N80 associated with transport over Norway, Sweden, Finland and Russia in the observations, which is replicated by both UKESM configurations at varying magnitudes. In ECHAM there is not sufficient transport from that region to facilitate comparison, however, in general we see an underprediction of N80 concentrations compared to the observations (Fig. S12j). The decrease in N80 is too negative in UKESM-BLN for transport from the South-East, which is associated with overprediction of N80 in the climatology and underprediction in 2014, for the organic-mediated BLN.

We find that for the boreal sites UKESM-BLN demonstrates the most consistent ΔN80 compared to observations and through Lagrangian analysis suggest that condensation and coagulation of new particles formed through enhanced BLN during the eruption, is resulting in the growth of the particles to larger diameters rather than increased concentrations. This is consistent with Jordan et al. (2025) which found that there was lower change in CDNC at cloud top for UKESM-BLN compared to UKESM across the North Atlantic, and supports their hypothesis that clouds in the UKESM-BLN simulations were less susceptible to increases in aerosol, due to the competition for condensable vapour from the newly nucleated particles. These results highlight the importance of the representation of nucleation processes to accurately represent changes to aerosol populations, and thus to constrain radiative forcing associated with ACI. However, the change in effective radius of the cloud droplets was found to be more accurate in UKESM1.0, despite the aerosol changes not being representative of observations. Thus, further investigation into the ACI processes is key to untangle the differences in cloud response. This demonstrates the importance of evaluation of the lifecycle to evaluate the representation of aerosol perturbations.

https://doi.org/10.5194/egusphere-2026-1043
Preprint. Discussion started: 11 May 2026


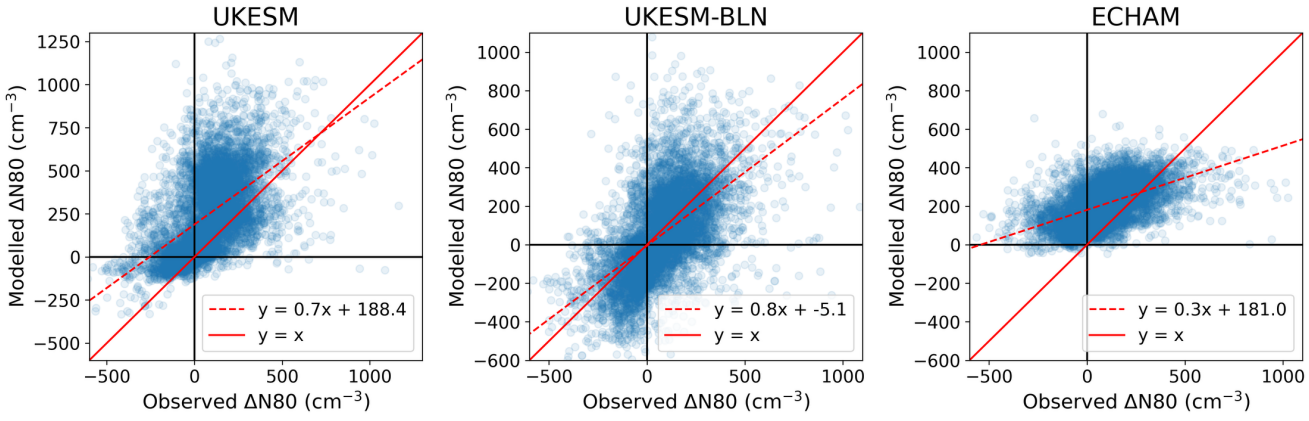


**Figure 14: The mean per grid cell for the difference (volcanic period minus climatology) in concentration, utilising the concentration weighted trajectory (CWT) model (Eq. 2, Fig. 13) for DMPS with ERA-Interim compared to UKESM1.0 (a), UKESM1.0-BLN10 (b) and ECHAM6.3-HAM2.3 (c). The solid red line indicates a 1:1 match and the dashed red line gives the regression between the two datasets. Note the difference in y-axis limits between subfigures, but consistent within subfigures.**

## 5 Conclusions

Volcanic plumes are routinely modelled in Lagrangian frameworks in operational dispersion models (e.g. Webster et al., 2012), and in this study Lagrangian methods have been used to evaluate deficiencies in bulk aerosol-related properties such as the initial vertical distribution of ash and $SO_2$ injection rates of explosive volcanic eruptions (De Leeuw et al., 2021). However, such frameworks have not been used in climate models to evaluate their performance and identify deficiencies in representation of complex microphysical processes. We have performed the first Lagrangian multi-model evaluation of the aerosol processes associated with an effusive volcanic perturbation.

Holuhraun had significant impact at the sites considered, demonstrating a consistent increase in the accumulation mode modal diameter across all three sites. The GCMs demonstrated substantial differences in their response. UKESM1.0 showed consistent increases in particle concentration, but not in modal diameter, which suggests gas-phase oxidation dominated, rather than aqueous phase oxidation, which would have only increased particle mass of the accumulation mode rather than the number for both modes. Additionally, the conversion from $SO_2$ to $SO_4$ was substantially slower for UKESM compared to ECHAM, where UKESM was closer to observations, which we suggest is associated with differences in the representation of oxidants and cloud pH.

The frequency of NPF events evident in the observational datasets and knowledge that nucleation is an important mediator of aerosol properties, motivated the inclusion of boundary layer nucleation into UKESM1.0, which had a significant impact on the response to the volcanic perturbation at the sites. With the inclusion of organic-mediated boundary layer nucleation,

https://doi.org/10.5194/egusphere-2026-1043
Preprint. Discussion started: 11 May 2026


UKESM-BLN was able to replicate the increase in accumulation mode diameter. However, total aerosol number concentrations were found to be on average a factor of 1.7 across the sites too high compared to observations. Despite concentrations of N80 for both the climatology and volcanic period being too high for UKESM-BLN, the perturbation (ΔN80) was best represented by this model for the boreal sites. ECHAM demonstrated the most accurate replication of the size distribution during the eruption period, however, the lack of accumulation mode particles in the climatology resulted in a too high perturbation, particularly associated with transport from Eastern Europe and Russia (Fig. 13j). The lack of nucleation and Aitken mode particles associated with transport from the eruption for ECHAM, highlights that the perturbation was associated with growth processes such as condensation and cloud processing, contributing to the mass of aerosol, rather than formation of new particles through gas phase oxidation. From observations at the boreal sites, there was evidence of sustained growth from NPF in the plume, which was not replicated by ECHAM, despite a lower condensation sink compared to the observations and UKESM variants, likely associated with the size of the particles when added to the nucleation mode limiting the number of particles transferred to the Aitken mode (Sporre et al., 2020).

PNSD measurements in the sub-10 nm range are subject to high counting uncertainties due to particle losses in DMPS measurement systems (Stolzenburg et al., 2023), thus we did not include analysis of the observations below 10nm. To further investigate the role of NPF in volcanic plumes, measurements of the nucleation mode particles are needed on the scale of a few nanometres. This would facilitate investigations studying NPF events and how these differ in an effusive eruption plume compared to the climatology, in particular through changes in particle formation and growth rates, as there have been few prior studies on NPF in volcanic plumes. Future work could also further investigate the evolution of the size distribution in GCMs through the Lagrangian framework by using a multiple in-situ measurement sites in a transport corridor, for example Abisko, Pallas and Värriö (Väänänen et al., 2013).

As noted in previous studies (e.g. Carslaw et al., 2013) the constraint on a baseline is key to be able to constrain the impact of a perturbation in ACI. In this study we have highlighted that the climatology aerosol size distribution is not well represented at the sites considered by the GCMs and thus represents a key avenue for constraining the impact of aerosol population. perturbations on cloud properties. Additionally, the ability to represent natural aerosol processes is crucial as feedbacks enhance natural aerosol processes, such as organic-mediated NPF, in warmer climates (Paasonen et al., 2013).

In this study we have investigated the perturbation in aerosol from the Holuhraun eruption to understand the change in potential CCN, however, to fully understand the impact on cloud properties, the sub-grid updraft would also be an important factor to consider, to obtain the impact of dynamics on CDNC. In an updraft limited regime, the activation of aerosol to cloud droplets depends on updraft velocity rather than aerosol number concentrations and has been found to vary significantly between GCMs (Reutter et al., 2009; Talvinen et al., 2025; Virtanen et al., 2025). This could be investigated in a Lagrangian framework in future work, to contribute further to understanding of the differences in cloud properties between GCMs.

https://doi.org/10.5194/egusphere-2026-1043
Preprint. Discussion started: 11 May 2026


In conclusion, our results have shown that GCMs differ greatly in their representation of the perturbation in aerosol size distribution resulting from an effusive volcanic eruption which have important implications for the representation of ACI. This opportunistic experiment highlights the importance of better understanding and improved model representations of natural aerosol processes to constrain the radiative forcing from aerosol cloud interactions, and the importance of performing a detailed assessment of the evolution of the aerosol particle size distribution to understand drivers of model differences. In particular, we have highlighted the critical role that BLN parameterisations play in modelling aerosol perturbations in the Arctic and Boreal regions, and further work remains to improve the representation of these processes across GCMs.

https://doi.org/10.5194/egusphere-2026-1043
Preprint. Discussion started: 11 May 2026


## Data availability

Field data (particle number size distributions) are freely available from the EBAS database at http://ebas.nilu.no/ (last access: 20 February 2022; NILU, 2022), full citations are described in Table S1. Details of $SO_2$ data are described in Table S2. The trajectories along with the collocated variables used in this study will be made available upon publication.

## Code availability

Python scripts used for the analysis and plotting will be made available upon publication. Python scripts for the data conversion (GCM output into ARL) and collocation of the GCM and reanalysis data variables to the trajectories can be obtained from DGP.

## Author contribution

DGP proposed the study. DGP, JMH, FM and EKD designed the research questions and simulations. BJ supported the setup for the configuration of the UKESM1 simulations performed as part the AeroCom GCM Trajectory experiment on which these simulations are based. GJ performed the UKESM simulations, and DW-P performed the ECHAM-HAM simulations. EKD processed the UKESM and ECHAM output with support from DGP, GJ, PK and DW-P. The modelling framework to calculate trajectories from GCM meteorological fields was conceived and developed by DGP with support from ZK and JT for ECHAM-HAM and UKESM respectively. Development of this framework for application to model output structure as defined from the AeroCom GCMTraj experiment was performed by PK with support from DGP, which EKD adapted and utilised in the study. ZK supported the processing of ERA-Interim reanalysis data. EKD prepared the in-situ measurement and GCM data, performed the trajectory calculations, analysed the simulation outputs and made the figures, with contributions from DGP, PK, JMH, AS, BJ, FM and GJ. The manuscript was written by EKD with contribution from DGP and JMH. All co-authors commented, edited and gave feedback on the manuscript.

## Competing interests

At least one of the (co-)authors is a member of the editorial board of Atmospheric Chemistry and Physics.

## Acknowledgements

We acknowledge use of the Monsoon2 system, a collaborative facility supplied under the Joint Weather and Climate Research Programme, a strategic partnership between the UK Met Office and the Natural Environment Research Council. We also thank all the people responsible for the development of UKESM and ECHAM.

We would also like to thank the technical and scientific staff at the in-situ measurement cites used in this study: Värriö, Pallas and Zeppelin. Data used in this study were accessed from EBAS (https://ebas.nilu.no) hosted by NILU. Specifically, the use included data affiliated with the frameworks: ACTRIS, GAW-WDCA, EMEP.

https://doi.org/10.5194/egusphere-2026-1043
Preprint. Discussion started: 11 May 2026


We would like to thank Ove Hermansen for providing the $SO_2$ observational dataset for Ny-Ålesund in September 2014. We would also like to thank Peter Tunved and Johan Ström for valuable discussion regarding the Zeppelin observational PNSD dataset.

DGP and JMH would like to extend personal thanks to Andy Jones, who provided support for the configuration of the UKESM simulations performed as part the AeroCom GCM Trajectory experiment on which these simulations are based.

**Financial support**

The work has been supported by the Centre for Doctoral Training in Environmental Intelligence: Data Science & AI for Sustainable Futures (grant no. EP/S022074/1) and the UK Met Office through a CASE PhD studentship. DGP has received partial support from NERC project (grant no. NE/T006331/1) and partial support from the Horizon Europe programme via project CleanCloud (Clouds and climate transitioning to post-fossil aerosol regime), grant agreement ID: 101137639. EKD, JMH, and DGP received partial funding from Quadrature Climate Foundation. JMH also received partial funding from SilverLining via their Safe Climate Research Initiative (SCRI). GJ acknowledges support from the European Union's Horizon 2020 CONSTRAIN grant (820829)

The ACTRIS project has received funding from the European Union's Horizon 2020 research and innovation programme under grant agreement No 654109.

https://doi.org/10.5194/egusphere-2026-1043
Preprint. Discussion started: 11 May 2026


## References

Alam, A., Shi, J. P., and Harrison, R. M.: Observations of new particle formation in urban air, Journal of Geophysical Research: Atmospheres, 108, https://doi.org/10.1029/2001JD001417, 2003.

EBAS Data Submission Manual: https://ebas-submit.nilu.no/templates/comments/fl_flag, last access: 17 December 2025.

Asmi, E., Kivekäs, N., Kerminen, V.-M., Komppula, M., Hyvärinen, A.-P., Hatakka, J., Viisanen, Y., and Lihavainen, H.: Secondary new particle formation in Northern Finland Pallas site between the years 2000 and 2010, Atmos. Chem. Phys, 11, 12959–12972, https://doi.org/10.5194/acp-11-12959-2011, 2011.

Beck, L. J., Sarnela, N., Junninen, H., Hoppe, C. J. M., Garmash, O., Bianchi, F., Riva, M., Rose, C., Peräkylä, O., Wimmer, D., Kausiala, O., Jokinen, T., Ahonen, L., Mikkilä, J., Hakala, J., He, X. C., Kontkanen, J., Wolf, K. K. E., Cappelletti, D., Mazzola, M., Traversi, R., Petroselli, C., Viola, A. P., Vitale, V., Lange, R., Massling, A., Nøjgaard, J. K., Krejci, R., Karlsson, L., Zieger, P., Jang, S., Lee, K., Vakkari, V., Lampilahti, J., Thakur, R. C., Leino, K., Kangasluoma, J., Duplissy, E. M., Siivola, E., Marbouti, M., Tham, Y. J., Saiz-Lopez, A., Petäjä, T., Ehn, M., Worsnop, D. R., Skov, H., Kulmala, M., Kerminen, V. M., and Sipilä, M.: Differing Mechanisms of New Particle Formation at Two Arctic Sites, Geophys. Res. Lett., 48, https://doi.org/10.1029/2020GL091334, 2021.

Bellouin, N., Rae, J., Jones, A., Johnson, C., Haywood, J., and Boucher, O.: Aerosol forcing in the Climate Model Intercomparison Project (CMIP5) simulations by HadGEM2-ES and the role of ammonium nitrate, Journal of Geophysical Research Atmospheres, 116, 20206, https://doi.org/10.1029/2011JD0160740, 2011.

Boichu, M., Favez, O., Riffault, V., Petit, J. E., Zhang, Y., Brogniez, C., Sciare, J., Chiapello, I., Clarisse, L., Zhang, S., Pujol-Söhne, N., Tison, E., Delbarre, H., and Goloub, P.: Large-scale particulate air pollution and chemical fingerprint of volcanic sulfate aerosols from the 2014-2015 Holuhraun flood lava eruption of Bárdarbunga volcano (Iceland), Atmos. Chem. Phys., 19, 14253–14287, https://doi.org/10.5194/ACP-19-14253-2019, 2019.

Boulon, J., Sellegri, K., Hervo, M., and Laj, P.: Observations of nucleation of new particles in a volcanic plume, Proc. Natl. Acad. Sci. U. S. A., 108, 12223–12226, https://doi.org/10.1073/PNAS.1104923108, 2011.

Bousiotis, D., Pope, F. D., Beddows, D. C. S., Dall'Osto, M., Massling, A., Nøjgaard, J. K., Nordstrøm, C., Niemi, J. V., Portin, H., Petäjä, T., Perez, N., Alastuey, A., Querol, X., Kouvarakis, G., Mihalopoulos, N., Vratolis, S., Eleftheriadis, K., Wiedensohler, A., Weinhold, K., Merkel, M., Tuch, T., and Harrison, R. M.: A phenomenology of new particle formation (NPF) at 13 European sites, Atmos. Chem. Phys., 21, 11905–11925, https://doi.org/10.5194/ACP-21-11905-2021, 2021.

Calvert, J. G., Su, F., Bottenheim, J. W., and Strausz, O. P.: Mechanism of the homogeneous oxidation of sulfur dioxide in the troposphere, Atmos. Environ., 12, 197–226, https://doi.org/10.1016/0004-6981(78)90201-9, 1978.

Carboni, E., Mather, T. A., Schmidt, A., Grainger, R. G., Pfeffer, M. A., Ialongo, I., and Theys, N.: Satellite-derived sulfur dioxide (SO2) emissions from the 2014-2015 Holuhraun eruption (Iceland), Atmos. Chem. Phys., 19, 4851–4862, https://doi.org/10.5194/ACP-19-4851-2019, 2019.

https://doi.org/10.5194/egusphere-2026-1043
Preprint. Discussion started: 11 May 2026


Carslaw, K. S., Lee, L. A., Reddington, C. L., Pringle, K. J., Rap, A., Forster, P. M., Mann, G. W., Spracklen, D. V., Woodhouse, M. T., Regayre, L. A., and Pierce, J. R.: Large contribution of natural aerosols to uncertainty in indirect forcing, Nature, 503, 67–71, https://doi.org/10.1038/nature12674, 2013.

Chen, Y., Haywood, J., Wang, Y., Malavelle, F., Jordan, G., Partridge, D., Fieldsend, J., De Leeuw, J., Schmidt, A., Cho, N., Oreopoulos, L., Platnick, S., Grosvenor, D., Field, P., and Lohmann, U.: Machine learning reveals climate forcing from aerosols is dominated by increased cloud cover, Nature Geoscience 2022 15:8, 15, 609–614, https://doi.org/10.1038/s41561-022-00991-6, 2022.

Christensen, M. W., Gettelman, A., Cermak, J., Dagan, G., Diamond, M., Douglas, A., Feingold, G., Glassmeier, F., Goren, T., Grosvenor, D. P., Gryspeerdt, E., Kahn, R., Li, Z., Ma, P. L., Malavelle, F., McCoy, I. L., McCoy, D. T., McFarquhar, G., Mülmenstädt, J., Pal, S., Possner, A., Povey, A., Quaas, J., Rosenfeld, D., Schmidt, A., Schrödner, R., Sorooshian, A., Stier, P., Toll, V., Watson-Parris, D., Wood, R., Yang, M., and Yuan, T.: Opportunistic experiments to constrain aerosol effective radiative forcing, Atmos. Chem. Phys., 22, 641–674, https://doi.org/10.5194/ACP-22-641-2022, 2022.

Croft, B., Martin, R. V., Richard Leaitch, W., Tunved, P., Breider, T. J., D'Andrea, S. D., and Pierce, J. R.: Processes controlling the annual cycle of Arctic aerosol number and size distributions, Atmos. Chem. Phys., 16, 3665–3682, https://doi.org/10.5194/ACP-16-3665-2016, 2016.

Dal Maso, M., Kulmala, M., Riipinen, I., Wagner, R., Hussein, T., Aalto, P. P., and Lehtinen, K. E. J.: Formation and growth of fresh atmospheric aerosols: eight years of aerosol size distribution data from SMEAR II, Hyytiälä, Finland, Boreal Environment Research, https://doi.org/10.60910/YQ6Q-VJ10, 2005.

Dal Maso, M., Sogacheva, L., Aalto, P. P., Riipinen, I., Komppula, M., Tunved, P., Korhonen, L., Suur-uski, V., Hirsikko, A., Kurtén, T., Kerminen, V. M., Lihavainen, H., Viisanen, Y., Hansson, H. C., and Kulmala, M.: Aerosol size distribution measurements at four Nordic field stations: identification, analysis and trajectory analysis of new particle formation bursts, Tellus B, 59, 350–361, https://doi.org/10.1111/J.1600-0889.2007.00267.X, 2007.

Dal Maso, M., Hyvärinen, A., Komppula, M., Tunved, P., Kerminen, V. M., Lihavainen, H., Viisanen, Y., Hansson, H. C., and Kulmala, M.: Annual and interannual variation in boreal forest aerosol particle number and volume concentration and their connection to particle formation, Tellus B Chem. Phys. Meteorol., 60, 495–508, https://doi.org/10.1111/J.1600-0889.2008.00366.X, 2008.

Dall'Osto, M., Beddows, D. C. S., Tunved, P., Krejci, R., Ström, J., Hansson, H. C., Yoon, Y. J., Park, K. T., Becagli, S., Udisti, R., Onasch, T., Ó'Dowd, C. D., Simó, R., and Harrison, R. M.: Arctic sea ice melt leads to atmospheric new particle formation, Scientific Reports 2017 7:1, 7, 1–10, https://doi.org/10.1038/s41598-017-03328-1, 2017.

Dee, D. P., Uppala, S. M., Simmons, A. J., Berrisford, P., Poli, P., Kobayashi, S., Andrae, U., Balmaseda, M. A., Balsamo, G., Bauer, P., Bechtold, P., Beljaars, A. C. M., van de Berg, L., Bidlot, J., Bormann, N., Delsol, C., Dragani, R., Fuentes, M., Geer, A. J., Haimberger, L., Healy, S. B., Hersbach, H., Hólm, E. V., Isaksen, L., Kållberg, P., Köhler, M., Matricardi, M., Mcnally, A. P., Monge-Sanz, B. M., Morcrette, J. J., Park, B. K., Peubey, C., de Rosnay, P., Tavolato, C., Thépaut, J. N., and

https://doi.org/10.5194/egusphere-2026-1043
Preprint. Discussion started: 11 May 2026


Vitart, F.: The ERA-Interim reanalysis: configuration and performance of the data assimilation system, Quarterly Journal of the Royal Meteorological Society, 137, 553–597, https://doi.org/10.1002/QJ.828, 2011.

Duncan, E. K., Fieldsend, J. E., Sellar, A., Tovazzi, E., Kim, P., Haywood, J. M., and Partridge, D. G.: A framework to holistically investigate processes controlling the aerosol lifecycle using explainable AI techniques, EGUsphere, 1–57, https://doi.org/10.5194/EGUSPHERE-2025-4298, 2025. [pre-print]

Engström, A. and Magnusson, L.: Estimating trajectory uncertainties due to flow dependent errors in the atmospheric analysis, Atmos. Chem. Phys., 9, 8857–8867, https://doi.org/10.5194/acp-9-8857-2009, 2009.

Faloona, I.: Sulfur processing in the marine atmospheric boundary layer: A review and critical assessment of modeling uncertainties, Atmos. Environ., 43, 2841–2854, https://doi.org/10.1016/J.ATMOSENV.2009.02.043, 2009.

Fritsch, F. N. and Butland, J.: A Method for Constructing Local Monotone Piecewise Cubic Interpolants, SIAM Journal on Scientific and Statistical Computing, 5, 300–304, https://doi.org/10.1137/0905021, 1984.

Fuchs, N. A. , and Sutugin, A. G.: High-Dispersed Aerosols, in: Topics in Current Aerosol Research, edited by: Hidy, G. M. and Brock, J. R. , Pergamon, New York, 1 pp., https://doi.org/10.1016/B978-0-08-016674-2.50006-6, 1971.

Ghan, S., Wang, M., Zhang, S., Ferrachat, S., Gettelman, A., Griesfeller, J., Kipling, Z., Lohmann, U., Morrison, H., Neubauer, D., Partridge, D. G., Stier, P., Takemura, T., Wang, H., and Zhang, K.: Challenges in constraining anthropogenic aerosol effects on cloud radiative forcing using present-day spatiotemporal variability, Proc. Natl. Acad. Sci. U. S. A., 113, 5804–5811, https://doi.org/10.1073/PNAS.1514036113, 2016.

von Glasow, R., Bobrowski, N., and Kern, C.: The effects of volcanic eruptions on atmospheric chemistry, Chem. Geol., 263, 131–142, https://doi.org/10.1016/J.CHEMGEO.2008.08.020, 2009.

Goto, D., Nakajima, T., Takemura, T., and Sudo, K.: Atmospheric Chemistry and Physics A study of uncertainties in the sulfate distribution and its radiative forcing associated with sulfur chemistry in a global aerosol model, Atmos. Chem. Phys, 11, 10889–10910, https://doi.org/10.5194/acp-11-10889-2011, 2011.

Haghighatnasab, M., Kretzschmar, J., Block, K., and Quaas, J.: Impact of Holuhraun volcano aerosols on clouds in cloud-system-resolving simulations, Atmos. Chem. Phys, 22, 8457–8472, https://doi.org/10.5194/acp-22-8457-2022, 2022.

Hardacre, C., Mulcahy, J. P., Pope, R. J., Jones, C. G., Rumbold, S. T., Li, C., Johnson, C., and Turnock, S. T.: Evaluation of SO2, SO42-and an updated SO2dry deposition parameterization in the United Kingdom Earth System Model, Atmos. Chem. Phys., 21, 18465–18497, https://doi.org/10.5194/ACP-21-18465-2021, 2021.

Hari, Pertti., Aalto, P., Hämeri, K., Kulmala, Markku., Lahti, Tapani., Luoma, Sari., Palva, L., Pohja, T., Pulliainen, Erkki., Siivola, Erkki., and Vesala, T.: Air pollution in eastern Lapland : challenge for an environmental measurement station., Silva Fennica, 28, 29–39, https://doi.org/10.14214/SF.A9160, 1994.

Hatakka, J., Aalto, T., Aaltonen, V., Aurela, M., Hakola, H., Komppula, M., Laurila, T., Lihavainen, H., Paatero, J., Salminen, K., and Viisanen, Y.: Overview of the atmospheric research activities and results at Pallas GAW station, 2003.

Hsu, Y. K., Holsen, T. M., and Hopke, P. K.: Comparison of hybrid receptor models to locate PCB sources in Chicago, Atmos. Environ., 37, 545–562, https://doi.org/10.1016/S1352-2310(02)00886-5, 2003.

https://doi.org/10.5194/egusphere-2026-1043
Preprint. Discussion started: 11 May 2026


Hussein, T., Junninen, H., Tunved, P., Kristensson, A., Dal Maso, M., Riipinen, I., Aalto, P. P., Hansson, H. C., Swietlicki, E., and Kulmala, M.: Time span and spatial scale of regional new particle formation events over Finland and Southern Sweden, Atmos. Chem. Phys., 9, 4699–4716, https://doi.org/10.5194/ACP-9-4699-2009, 2009.

Ilyinskaya, E., Schmidt, A., Mather, T. A., Pope, F. D., Witham, C., Baxter, P., Jóhannsson, T., Pfeffer, M., Barsotti, S., Singh, A., Sanderson, P., Bergsson, B., McCormick Kilbride, B., Donovan, A., Peters, N., Oppenheimer, C., and Edmonds, M.: Understanding the environmental impacts of large fissure eruptions: Aerosol and gas emissions from the 2014–2015 Holuhraun eruption (Iceland), Earth Planet. Sci. Lett., 472, 309–322, https://doi.org/10.1016/J.EPSL.2017.05.025, 2017.

Inness, A., Baier, F., Benedetti, A., Bouarar, I., Chabrillat, S., Clark, H., Clerbaux, C., Coheur, P., Engelen, R. J., Errera, Q., Flemming, J., George, M., Granier, C., Hadji-Lazaro, J., Huijnen, V., Hurtmans, D., Jones, L., Kaiser, J. W., Kapsomenakis, J., Lefever, K., Leitão, J., Razinger, M., Richter, A., Schultz, M. G., Simmons, A. J., Suttie, M., Stein, O., Thépaut, J. N., Thouret, V., Vrekoussis, M., and Zerefos, C.: The MACC reanalysis: An 8 yr data set of atmospheric composition, Atmos. Chem. Phys., 13, 4073–4109, https://doi.org/10.5194/ACP-13-4073-2013, 2013.

Jordan, G., Malavelle, F., Chen, Y., Peace, A., Duncan, E., Partridge, D. G., Kim, P., Watson-Parris, D., Takemura, T., Neubauer, D., Myhre, G., Skeie, R., Laakso, A., and Haywood, J.: How well are aerosol-cloud interactions represented in climate models? - Part 1: Understanding the sulfate aerosol production from the 2014-15 Holuhraun eruption, Atmos. Chem. Phys., 24, 1939–1960, https://doi.org/10.5194/ACP-24-1939-2024, 2024.

Jordan, G., Malavelle, F., Haywood, J., Chen, Y., Johnson, B., Partridge, D., Peace, A., Duncan, E., Watson-Parris, D., Neubauer, D., Laakso, A., Michou, M., and Nabat, P.: How well are aerosol–cloud interactions represented in climate models? – Part 2: Isolating the aerosol impact on clouds following the 2014–2015 Holuhraun eruption, Atmos. Chem. Phys., 25, 13393–13428, https://doi.org/10.5194/ACP-25-13393-2025, 2025.

K. Sporre, M., M. Blichner, S., Schrödner, R., H. H. Karset, I., K. Berntsen, T., Van Noije, T., Bergman, T., O'Donnell, D., and Makkonen, R.: Large difference in aerosol radiative effects from BVOC-SOA treatment in three Earth system models, Atmos. Chem. Phys., 20, 8953–8973, https://doi.org/10.5194/ACP-20-8953-2020, 2020.

Karset, I. H. H., Koren Berntsen, T., Storelvmo, T., Alterskjær, K., Grini, A., Olivié, Di., Kirkeväg, A., Seland, Ø., Iversen, T., and Schulz, M.: Strong impacts on aerosol indirect effects from historical oxidant changes, Atmos. Chem. Phys., 18, 7669–7690, https://doi.org/10.5194/ACP-18-7669-2018, 2018.

Kazil, J., Stier, P., Zhang, K., Quaas, J., Kinne, S., O'Donnell, D., Rast, S., Esch, M., Ferrachat, S., Lohmann, U., and Feichter, J.: Aerosol nucleation and its role for clouds and Earth's radiative forcing in the aerosol-climate model ECHAM5-HAM, Atmos. Chem. Phys., 10, 10733–10752, https://doi.org/10.5194/ACP-10-10733-2010, 2010.

Kerminen, V. M. and Kulmala, M.: Analytical formulae connecting the "real" and the "apparent" nucleation rate and the nuclei number concentration for atmospheric nucleation events, J. Aerosol Sci., 33, 609–622, https://doi.org/10.1016/S0021-8502(01)00194-X, 2002.

Kerminen, V.-M., Kerminen, V.-M., Paramonov, M., Anttila, T., Riipinen, I., Fountoukis, C., Korhonen, H., Asmi, E., Laakso, L., Lihavainen, H., Swietlicki, E., Svenningsson, B., Asmi, A., Pandis, S. N., Kulmala, M., and Petäjä, T.: Cloud condensation

https://doi.org/10.5194/egusphere-2026-1043
Preprint. Discussion started: 11 May 2026


nuclei production associated with atmospheric nucleation: a synthesis based on existing literature and new results, Atmos. Chem. Phys., 12, 12037–12059, https://doi.org/10.5194/acp-12-12037-2012, 2012.

Kim, P., Partridge, D., and Haywood, J.: Constraining the model representation of the aerosol life cycle in relation to sources and sinks., in: 22nd EGU General Assembly, 21948, https://doi.org/10.5194/EGUSPHERE-EGU2020-21948, 2020.

Komppula, M., Sihto, S.-L., Korhonen, H., Lihavainen, H., Kerminen, V.-M., Kulmala, M., and Viisanen, Y.: New particle formation in air mass transported between two measurement sites in Northern Finland, Atmos. Chem. Phys, 6, 2824, 2006.

Korhola, T., Kokkola, H., Korhonen, H., Laaksonen, A., Lehtinen, K. E. J., and Romakkaniemi, S.: Reallocation in modal aerosol models: Impacts on predicting aerosol radiative effects, Geosci. Model Dev., 7, 161–174, https://doi.org/10.5194/GMD-7-161-2014, 2014.

Kreidenweis, S. M., Walcek, C. J., Feingold, G., Gong, W., Jacobson, M. Z., Kim, C.-H., Liu, X., Penner, J. E., Nenes, A., Seinfeld, J. H., Walcek, C. M. J., Feingold, G., Gong, W., Jacobson, M. Z., Kim, C.-H., Liu, X., Penner, J. E., Nenes, A., and Seinfeld, J. H.: Modification of aerosol mass and size distribution due to aqueous-phase SO2 oxidation in clouds: Comparisons of several models, Journal of Geophysical Research: Atmospheres, 108, 4213, https://doi.org/10.1029/2002JD002697, 2003.

Kulmala, M., Dal Maso, M., Mäkelä, J. M., Pirjola, L., Väkevä, M., Aalto, P., Miikkulainen, P., Hämeri, K., and O'Dowd, C. D.: On the formation, growth and composition of nucleation mode particles, Tellus B Chem. Phys. Meteorol., 53, 479–490, https://doi.org/10.3402/tellusb.v53i4.16622, 2001.

Kyrö, E.-M., Väänänen, R., Kerminen, V.-M., Virkkula, A., Petäjä, T., Asmi, A., Dal Maso, M., Nieminen, T., Juhola, S., Shcherbinin, A., Riipinen, I., Lehtipalo, K., Keronen, P., Aalto, P. P., Hari, P., and Kulmala, M.: Atmospheric Chemistry and Physics Trends in new particle formation in eastern Lapland, Finland: effect of decreasing sulfur emissions from Kola Peninsula, Atmos. Chem. Phys, 14, 4383–4396, https://doi.org/10.5194/acp-14-4383-2014, 2014.

Lee, H., Lee, K., Rene Lunder, C., Krejci, R., Aas, W., Park, J., Park, K. T., Yong Lee, B., Yoon, Y. J., and Park, K.: Atmospheric new particle formation characteristics in the Arctic as measured at Mount Zeppelin, Svalbard, from 2016 to 2018, Atmos. Chem. Phys., 20, 13425–13441, https://doi.org/10.5194/ACP-20-13425-2020, 2020.

De Leeuw, J., Schmidt, A., Witham, C. S., Theys, N., Taylor, I. A., Grainger, R. G., Pope, R. J., Haywood, J., Osborne, M., and Kristiansen, N. I.: The 2019 Raikoke volcanic eruption - Part 1: Dispersion model simulations and satellite retrievals of volcanic sulfur dioxide, Atmos. Chem. Phys., 21, 10851–10879, https://doi.org/10.5194/ACP-21-10851-2021, 2021.

Malavelle, F. F., Haywood, J. M., Jones, A., Gettelman, A., Clarisse, L., Bauduin, S., Allan, R. P., Karset, I. H. H., Kristjánsson, J. E., Oreopoulos, L., Cho, N., Lee, D., Bellouin, N., Boucher, O., Grosvenor, D. P., Carslaw, K. S., Dhomse, S., Mann, G. W., Schmidt, A., Coe, H., Hartley, M. E., Dalvi, M., Hill, A. A., Johnson, B. T., Johnson, C. E., Knight, J. R., O'Connor, F. M., Stier, P., Myhre, G., Platnick, S., Stephens, G. L., Takahashi, H., and Thordarson, T.: Strong constraints on aerosol–cloud interactions from volcanic eruptions, Nature 2017 546:7659, 546, 485–491, https://doi.org/10.1038/nature22974, 2017.

Mann, G. W., Carslaw, K. S., Spracklen, D. V, Ridley, D. A., Manktelow, P. T., Chipperfield, M. P., Pickering, S. J., and Johnson, C. E.: Geoscientific Model Development Description and evaluation of GLOMAP-mode: a modal global aerosol

microphysics model for the UKCA composition-climate model, Geosci. Model Dev, 3, 519–551, https://doi.org/10.5194/gmd-3-519-2010, 2010.

Manninen, H. E., Nieminen, T., Asmi, E., Gagné, S., Häkkinen, S., Lehtipalo, K., Aalto, P., Vana, M., Mirme, A., Mirme, S., Hõrrak, U., Plass-D ¨ Ulmer, C., Stange, G., Kiss, G., Hoffer, A., Tör″, N., Moerman, M., Henzing, B., De Leeuw, G., Brinkenberg, M., Kouvarakis, G. N., Bougiatioti, A., Mihalopoulos, N., O'dowd, C., Ceburnis, D., Arneth, A., Svenningsson, B., Swietlicki, E., Tarozzi, L., Decesari, S., Facchini, M. C., Birmili, W., Sonntag, A., Wiedensohler, A., Boulon, J., Sellegri, K., Laj, P., Gysel, M., Bukowiecki, N., Weingartner, E., Wehrle, G., Laaksonen, A., Hamed, A., Joutsensaari, J., Petäjä, T., Kerminen, V.-M., and Kulmala, M.: Atmospheric Chemistry and Physics EUCAARI ion spectrometer measurements at 12 European sites-analysis of new particle formation events, Atmos. Chem. Phys, 10, 7907–7927, https://doi.org/10.5194/acp-10-7907-2010, 2010.

Marelle, L., Myhre, G., Thomas, J. L., and Raut, J. C.: Aerosol Background Concentrations Influence Aerosol-Cloud Interactions as Much as the Choice of Aerosol-Cloud Parameterization, Geophys. Res. Lett., 52, e2024GL111780, https://doi.org/10.1029/2024GL111780, 2025.

McCoy, D. T. and Hartmann, D. L.: Observations of a substantial cloud-aerosol indirect effect during the 2014–2015 Bárðarbunga-Veiðivötn fissure eruption in Iceland, Geophys. Res. Lett., 42, 10,409-10,414, https://doi.org/10.1002/2015GL067070, 2015.

Metzger, A., Verheggen, B., Dommen, J., Duplissy, J., Prevot, A. S. H., Weingartner, E., Riipinen, I., Kulmala, M., Spracklen, D. V., Carslaw, K. S., and Baltensperger, U.: Evidence for the role of organics in aerosol particle formation under atmospheric conditions, Proc. Natl. Acad. Sci. U. S. A., 107, 6646–6651, https://doi.org/10.1073/PNAS.0911330107, 2010.

Mulcahy, J. P., Johnson, C., Jones, C. G., Povey, A. C., Scott, C. E., Sellar, A., Turnock, S. T., Woodhouse, M. T., Abraham, N. L., Andrews, M. B., Bellouin, N., Browse, J., Carslaw, K. S., Dalvi, M., Folberth, G. A., Glover, M., Grosvenor, D. P., Hardacre, C., Hill, R., Johnson, B., Jones, A., Kipling, Z., Mann, G., Mollard, J., O'Connor, F. M., Palmiéri, J., Reddington, C., Rumbold, S. T., Richardson, M., Schutgens, N. A. J., Stier, P., Stringer, M., Tang, Y., Walton, J., Woodward, S., and Yool, A.: Description and evaluation of aerosol in UKESM1 and HadGEM3-GC3.1 CMIP6 historical simulations, Geosci. Model Dev., 13, 6383–6423, https://doi.org/10.5194/GMD-13-6383-2020, 2020.

Paasonen, P., Asmi, A., Petäjä, T., Kajos, M. K., Äijälä, M., Junninen, H., Holst, T., Abbatt, J. P. D., Arneth, A., Birmili, W., Van Der Gon, H. D., Hamed, A., Hoffer, A., Laakso, L., Laaksonen, A., Richard Leaitch, W., Plass-Dülmer, C., Pryor, S. C., Räisänen, P., Swietlicki, E., Wiedensohler, A., Worsnop, D. R., Kerminen, V. M., and Kulmala, M.: Warming-induced increase in aerosol number concentration likely to moderate climate change, Nature Geoscience 2013 6:6, 6, 438–442, https://doi.org/10.1038/ngeo1800, 2013.

Peace, A. H., Chen, Y., Jordan, G., Partridge, D. G., Malavelle, F., Duncan, E., and Haywood, J. M.: In-plume and out-of-plume analysis of aerosol–cloud interactions derived from the 2014–2015 Holuhraun volcanic eruption, Atmos. Chem. Phys., 24, 9533–9553, https://doi.org/10.5194/ACP-24-9533-2024, 2024.

https://doi.org/10.5194/egusphere-2026-1043
Preprint. Discussion started: 11 May 2026


Pernov, J. B., Harris, E., Volpi, M., Baumgartner, T., Hohermuth, B., Empa, S. H., Aeberhard, W. H., Becagli, S., Quinn, P. K., Traversi, R., Upchurch, L. M., and Schmale, J.: Pan-Arctic Methanesulfonic Acid Aerosol: Source regions, atmospheric drivers, and future projections, https://doi.org/10.21203/RS.3.RS-3976619/V1, 2024.

Price, R., Baccarini, A., Schmale, J., Zieger, P., Brooks, I. M., Field, P., and Carslaw, K. S.: Late summer transition from a free-Tropospheric to boundary layer source of Aitken mode aerosol in the high Arctic, Atmos. Chem. Phys., 23, 2927–2961, https://doi.org/10.5194/ACP-23-2927-2023, 2023.

Ranjithkumar, A., Gordon, H., Williamson, C., Rollins, A., Pringle, K., Kupc, A., Luke Abraham, N., Brock, C., and Carslaw, K.: Constraints on global aerosol number concentration, SO2and condensation sink in UKESM1 using ATom measurements, Atmos. Chem. Phys., 21, 4979–5014, https://doi.org/10.5194/ACP-21-4979-2021, 2021.

Reutter, P., Su, H., Trentmann, J., Simmel, M., Rose, D., Gunthe, S. S., Wernli, H., Andreae, M. O., and Pöschl, U.: Aerosol- and updraft-limited regimes of cloud droplet formation: Influence of particle number, size and hygroscopicity on the activation of cloud condensation nuclei (CCN), Atmos. Chem. Phys., 9, 7067–7080, https://doi.org/10.5194/ACP-9-7067-2009, 2009.

Roelofs, G. J., Stier, P., Feichter, J., Vignati, E., and Wilson, J.: Atmospheric Chemistry and Physics Aerosol activation and cloud processing in the global aerosol-climate model ECHAM5-HAM, Atmos. Chem. Phys, 6, 2389–2399, 2006.

Rose, C., Foucart, B., Picard, D., Colomb, A., Metzger, J. M., Tulet, P., and Sellegri, K.: New particle formation in the volcanic eruption plume of the Piton de la Fournaise: Specific features from a long-term dataset, Atmos. Chem. Phys., 19, 13243–13265, https://doi.org/10.5194/ACP-19-13243-2019, 2019.

Sahyoun, M., Freney, E., Brito, J., Duplissy, J., Gouhier, M., Colomb, A., Dupuy, R., Bourianne, T., Nowak, J. B., Yan, C., Petäjä, T., Kulmala, M., Schwarzenboeck, A., Planche, C., and Sellegri, K.: Evidence of New Particle Formation Within Etna and Stromboli Volcanic Plumes and Its Parameterization From Airborne In Situ Measurements, Journal of Geophysical Research: Atmospheres, 124, 5650–5668, https://doi.org/10.1029/2018JD028882, 2019.

Schmidt, A., Leadbetter, S., Theys, N., Carboni, E., Witham, C. S., Stevenson, J. A., Birch, C. E., Thordarson, T., Turnock, S., Barsotti, S., Delaney, L., Feng, W., Grainger, R. G., Hort, M. C., Höskuldsson, Á., Ialongo, I., Ilyinskaya, E., Jóhannsson, T., Kenny, P., Mather, T. A., Richards, N. A. D., and Shepherd, J.: Satellite detection, long-range transport, and air quality impacts of volcanic sulfur dioxide from the 2014–2015 flood lava eruption at Bárðarbunga (Iceland), Journal of Geophysical Research: Atmospheres, 120, 9739–9757, https://doi.org/10.1002/2015JD023638, 2015.

Seinfeld, J. H. and Pandis, S. N.: Atmospheric chemistry and physics from air pollution to climate change, 2nd ed., Wiley-Interscience, New York, 2006.

Seinfeld, J. H. and Pandis, S. N.: Atmospheric Chemistry and Physics: From Air Pollution to Climate Change, 2nd ed., John Wiley and Sons, New Jersey, 2012.

Sellar, A. A., Jones, C. G., Mulcahy, J. P., Tang, Y., Yool, A., Wiltshire, A., O'Connor, F. M., Stringer, M., Hill, R., Palmieri, J., Woodward, S., de Mora, L., Kuhlbrodt, T., Rumbold, S. T., Kelley, D. I., Ellis, R., Johnson, C. E., Walton, J., Abraham, N. L., Andrews, M. B., Andrews, T., Archibald, A. T., Berthou, S., Burke, E., Blockley, E., Carslaw, K., Dalvi, M., Edwards, J., Folberth, G. A., Gedney, N., Griffiths, P. T., Harper, A. B., Hendry, M. A., Hewitt, A. J., Johnson, B., Jones, A., Jones, C. D.,

https://doi.org/10.5194/egusphere-2026-1043
Preprint. Discussion started: 11 May 2026


Keeble, J., Liddicoat, S., Morgenstern, O., Parker, R. J., Predoi, V., Robertson, E., Siahaan, A., Smith, R. S., Swaminathan, R., Woodhouse, M. T., Zeng, G., and Zerroukat, M.: UKESM1: Description and Evaluation of the U.K. Earth System Model, J. Adv. Model. Earth Syst., 11, 4513–4558, https://doi.org/10.1029/2019MS001739, 2019.

Sigmundsson, F., Hooper, A., Hreinsdóttir, S., Vogfjörd, K. S., Ófeigsson, B. G., Heimisson, E. R., Dumont, S., Parks, M., Spaans, K., Gudmundsson, G. B., Drouin, V., Árnadóttir, T., Jónsdóttir, K., Gudmundsson, M. T., Högnadóttir, T., Fridriksdóttir, H. M., Hensch, M., Einarsson, P., Magnússon, E., Samsonov, S., Brandsdóttir, B., White, R. S., Ágústsdóttir, T., Greenfield, T., Green, R. G., Hjartardóttir, Á. R., Pedersen, R., Bennett, R. A., Geirsson, H., la Femina, P. C., Björnsson, H., Pálsson, F., Sturkell, E., Bean, C. J., Möllhoff, M., Braiden, A. K., and Eibl, E. P. S.: Segmented lateral dyke growth in a rifting event at Bárðarbunga volcanic system, Iceland, Nature, 517, 191–195, https://doi.org/10.1038/nature14111, 2015.

Sogacheva, L., Dal Maso, M., Kerminen, V.-M., and Kulmala, M.: Probability of nucleation events and aerosol particle concentration in different air mass types arriving at Hyytiälä, southern Finland, based on back trajectories analysis., Boreal Environment Research, 479–491, 2005.

Spracklen, D. v, Pringle, K. J., Carslaw, K. S., Chipperfield, M. P., and Mann, G. W.: Atmospheric Chemistry and Physics A global off-line model of size-resolved aerosol microphysics: I. Model development and prediction of aerosol properties, Atmos. Chem. Phys, 2227–2252 pp., 2005.

Spracklen, D. V., Bonn, B., and Carslaw, K. S.: Boreal forests, aerosols and the impacts on clouds and climate, Philosophical Transactions of the Royal Society A: Mathematical, Physical and Engineering Sciences, 366, 4613–4626, https://doi.org/10.1098/RSTA.2008.0201, 2008.

Stein, A. F., Draxler, R. R., Rolph, G. D., Stunder, B. J. B., Cohen, M. D., and Ngan, F.: Noaa's hysplit atmospheric transport and dispersion modeling system, https://doi.org/10.1175/BAMS-D-14-00110.1, 1 December 2015.

Stier, P., Feichter, J., Kinne, S., Kloster, S., Vignati, E., Wilson, J., Ganzeveld, L., Tegen, I., Werner, M., Balkanski, Y., Schulz, M., Boucher, O., Minikin, A., and Petzold, A.: The aerosol-climate model ECHAM5-HAM, Atmos. Chem. Phys., 5, 1125–1156, https://doi.org/10.5194/ACP-5-1125-2005, 2005.

Stockwell, W. R. and Calvert, J. G.: The mechanism of the HO-SO2 reaction, Atmospheric Environment (1967), 17, 2231–2235, https://doi.org/10.1016/0004-6981(83)90220-2, 1983.

Stolzenburg, D., Laurila, T., Aalto, P., Vanhanen, J., Petäjä, T., and Kangasluoma, J.: Improved counting statistics of an ultrafine differential mobility particle size spectrometer system, Atmos. Meas. Tech., 16, 2471–2483, https://doi.org/10.5194/AMT-16-2471-2023, 2023.

Ström, J., Umegård, J., Tørseth, K., Tunved, P., Hansson, H. C., Holmén, K., Wismann, V., Herber, A., and König-Langlo, G.: One year of particle size distribution and aerosol chemical composition measurements at the Zeppelin Station, Svalbard, March 2000-March 2001, Physics and Chemistry of the Earth, 28, 1181–1190, https://doi.org/10.1016/j.pce.2003.08.058, 2003.

https://doi.org/10.5194/egusphere-2026-1043
Preprint. Discussion started: 11 May 2026


Su, P., Joutsensaari, J., Dada, L., Zaidan, M. A., Nieminen, T., Li, X., Wu, Y., Decesari, S., Tarkoma, S., Petäjä, T., Kulmala, M., and Pellikka, P.: New particle formation event detection with Mask R-CNN, Atmos. Chem. Phys., 22, 1293–1309, https://doi.org/10.5194/ACP-22-1293-2022, 2022.

Svenhag, C., Roldin, P., Olenius, T., De Jonge, R. W., Blichner, S. M., Yazgi, D., and Sporre, M. K.: Seasonal differences in observed versus modelled new particle formation at two European boreal stations, Atmos. Chem. Phys., 25, 11483–11504, https://doi.org/10.5194/ACP-25-11483-2025, 2025.

Talvinen, S., Kim, P., Tovazzi, E., Holopainen, E., Cremer, R., Kühn, T., Kokkola, H., Kipling, Z., Neubauer, D., Teixeira, J. C., Sellar, A., Watson-Parris, D., Yang, Y., Zhu, J., Krishnan, S., Virtanen, A., and Partridge, D. G.: Towards an improved understanding of the impact of clouds and precipitation on the representation of aerosols over the Boreal Forest in GCMs, Atmos. Chem. Phys., 25, 14449–14478, https://doi.org/10.5194/ACP-25-14449-2025, 2025.

Tegen, I., Neubauer, D., Ferrachat, S., Drian, C. S. Le, Bey, I., Schutgens, N., Stier, P., Watson-Parris, D., Stanelle, T., Schmidt, H., Rast, S., Kokkola, H., Schultz, M., Schroeder, S., Daskalakis, N., Barthel, S., Heinold, B., and Lohmann, U.: The global aerosol-climate model echam6.3-ham2.3 -Part 1: Aerosol evaluation, Geosci. Model Dev., 12, 1643–1677, https://doi.org/10.5194/GMD-12-1643-2019, 2019.

Textor, C., Schulz, M., Guibert, S., Kinne, S., Balkanski, Y., Bauer, S., Berntsen, T., Berglen, T., Boucher, O., Chin, M., Dentener, F., Diehl, T., Easter, R., Feichter, H., Fillmore, D., Ghan, S., Ginoux, P., Gong, S., Grini, A., Hendricks, J., Horowitz, L., Huang, P., Isaksen, I., Iversen, T., Kloster, S., Koch, D., Kirkevåg, A., Kristjansson, J. E., Krol, M., Lauer, A., Lamarque, J. F., Liu, X., Montanaro, V., Myhre, G., Penner, J., Pitari, G., Reddy, S., Seland, Stier, P., Takemura, T., and Tie, X.: Analysis and quantification of the diversities of aerosol life cycles within AeroCom, Atmos. Chem. Phys., 6, 1777–1813, https://doi.org/10.5194/ACP-6-1777-2006, 2006.

Tröstl, J., Herrmann, E., Frege, C., Bianchi, F., Molteni, U., Bukowiecki, N., Hoyle, C. R., Steinbacher, M., Weingartner, E., Dommen, J., Gysel, M., and Baltensperger, U.: Contribution of new particle formation to the total aerosol concentration at the high-altitude site Jungfraujoch (3580masl, Switzerland), J. Geophys. Res., 121, 11692–11711, https://doi.org/10.1002/2015JD024637, 2016.

Tunved, P., Hansson, H.-C., Kulmala, M., Aalto, P., Viisanen, Y., Karlsson, H., Kristensson, A., Swietlicki, E., Dal Maso, M., Ström, J., and Komppula, M.: One year boundary layer aerosol size distribution data from five nordic background stations, Atmos. Chem. Phys, 3, 2183–2205, 2003.

Tunved, P., Hansson, H. C., Kerminen, V. M., Ström, J., Dal Maso, M., Lihavainen, H., Viisanen, Y., Aalto, P. P., Komppula, M., and Kulmala, M.: High natural aerosol loading over boreal forests, Science (1979)., 312, 261–263, https://doi.org/10.1126/science.1123052, 2006.

Tunved, P., Ström, J., and Krejci, R.: Arctic aerosol life cycle: Linking aerosol size distributions observed between 2000 and 2010 with air mass transport and precipitation at Zeppelin station, Ny-Ålesund, Svalbard, Atmos. Chem. Phys., 13, 3643–3660, https://doi.org/10.5194/acp-13-3643-2013, 2013.

https://doi.org/10.5194/egusphere-2026-1043
Preprint. Discussion started: 11 May 2026


Turnock, S. T., Mann, G. W., Woodhouse, M. T., Dalvi, M., O'Connor, F. M., Carslaw, K. S., and Spracklen, D. V.: The Impact of Changes in Cloud Water pH on Aerosol Radiative Forcing, Geophys. Res. Lett., 46, 4039–4048, https://doi.org/10.1029/2019GL082067, 2019.

Twigg, M., Ilyinskaya, E., Beccaceci, S., Green, D., Jones, M., Langford, B., Leeson, S., Lingard, J., Pereira, G., Carter, H., Poskitt, J., Richter, A., Ritchie, S., Simmons, I., Smith, R., Sim Tang, Y., Van Dijk, N., Vincent, K., Nemitz, E., Vieno, M., and Braban, C.: Impacts of the 2014-2015 Holuhraun eruption on the UK atmosphere, Atmos. Chem. Phys., 16, 11415–11431, https://doi.org/10.5194/ACP-16-11415-2016, 2016.

Väänänen, R., Kyrö, E. M., Kivekäs, N., Junninen, H., Virkkula, A., Dal Maso, M., Lihavainen, H., Viisanen, Y., Svenningsson, B., Holst, T., Arneth, A., Aalto, P. P., Kulmala, M., and Kerminen, V. M.: Analysis of particle size distribution changes between three measurement sites in northern Scandinavia, Atmos. Chem. Phys., 13, 11887–11903, https://doi.org/10.5194/acp-13-11887-2013, 2013.

Vehkamäki, H., Kulmala, M., Napari, I., Lehtinen, K. E. J., Timmreck, C., Noppel, M., and Laaksonen, A.: An improved parameterization for sulfuric acid–water nucleation rates for tropospheric and stratospheric conditions, Journal of Geophysical Research: Atmospheres, 107, AAC 3-1, https://doi.org/10.1029/2002JD002184, 2002.

Vehkamäki, H., Dal Maso, M., Hussein, T., Flanagan, R., Hyvärinen, A., Lauros, J., Merikanto, J., Mönkkönen, P., Pihlatie, M., Salminen, K., Sogacheva, L., Thum, T., Ruuskanen, T. M., Keronen, P., Aalto, P. P., Hari, P., Lehtinen, K. E. J., Rannik, ¨ U, and Kulmala, M.: Atmospheric Chemistry and Physics Atmospheric particle formation events at Värriö measurement station in Finnish Lapland 1998-2002, Atmos. Chem. Phys, 4, 2015.

Virtanen, A., Joutsensaari, J., Kokkola, H., Partridge, D. G., Blichner, S., Seland, Ø., Holopainen, E., Tovazzi, E., Lipponen, A., Mikkonen, S., Leskinen, A., Hyvärinen, A. P., Zieger, P., Krejci, R., Ekman, A. M. L., Riipinen, I., Quaas, J., and Romakkaniemi, S.: High sensitivity of cloud formation to aerosol changes, Nat. Geosci., 18, 289–295, https://doi.org/10.1038/S41561-025-01662-Y, 2025.

Virtanen, P., Gommers, R., Oliphant, T. E., Haberland, M., Reddy, T., Cournapeau, D., Burovski, E., Peterson, P., Weckesser, W., Bright, J., van der Walt, S. J., Brett, M., Wilson, J., Millman, K. J., Mayorov, N., Nelson, A. R. J., Jones, E., Kern, R., Larson, E., Carey, C. J., Polat, İ., Feng, Y., Moore, E. W., VanderPlas, J., Laxalde, D., Perktold, J., Cimrman, R., Henriksen, I., Quintero, E. A., Harris, C. R., Archibald, A. M., Ribeiro, A. H., Pedregosa, F., van Mulbregt, P., Vijaykumar, A., Bardelli, A. Pietro, Rothberg, A., Hilboll, A., Kloeckner, A., Scopatz, A., Lee, A., Rokem, A., Woods, C. N., Fulton, C., Masson, C., Häggström, C., Fitzgerald, C., Nicholson, D. A., Hagen, D. R., Pasechnik, D. V., Olivetti, E., Martin, E., Wieser, E., Silva, F., Lenders, F., Wilhelm, F., Young, G., Price, G. A., Ingold, G. L., Allen, G. E., Lee, G. R., Audren, H., Probst, I., Dietrich, J. P., Silterra, J., Webber, J. T., Slavič, J., Nothman, J., Buchner, J., Kulick, J., Schönberger, J. L., de Miranda Cardoso, J. V., Reimer, J., Harrington, J., Rodríguez, J. L. C., Nunez-Iglesias, J., Kuczynski, J., Tritz, K., Thoma, M., Newville, M., Kümmerer, M., Bolingbroke, M., Tartre, M., Pak, M., Smith, N. J., Nowaczyk, N., Shebanov, N., Pavlyk, O., Brodtkorb, P. A., Lee, P., McGibbon, R. T., Feldbauer, R., Lewis, S., Tygier, S., Sievert, S., Vigna, S., Peterson, S., More, S., Pudlik, T., et

https://doi.org/10.5194/egusphere-2026-1043
Preprint. Discussion started: 11 May 2026


al.: SciPy 1.0: fundamental algorithms for scientific computing in Python, Nature Methods 2020 17:3, 17, 261–272, https://doi.org/10.1038/s41592-019-0686-2, 2020.

Watson-Parris, D., Schutgens, N., Cook, N., Kipling, Z., Kershaw, P., Gryspeerdt, E., Lawrence, B., and Stier, P.: Community Intercomparison Suite (CIS) v1.4.0: A tool for intercomparing models and observations, Geosci. Model Dev., 9, 3093–3110, https://doi.org/10.5194/GMD-9-3093-2016, 2016.

Webster, H. N., Thomson, D. J., Johnson, B. T., Heard, I. P. C., Turnbull, K., Marenco, F., Kristiansen, N. I., Dorsey, J., Minikin, A., Weinzierl, B., Schumann, U., Sparks, R. S. J., Loughlin, S. C., Hort, M. C., Leadbetter, S. J., Devenish, B. J., Manning, A. J., Witham, C. S., Haywood, J. M., and Golding, B. W.: Operational prediction of ash concentrations in the distal volcanic cloud from the 2010 Eyjafjallajökull eruption, Journal of Geophysical Research: Atmospheres, 117, 0–08, https://doi.org/10.1029/2011JD016790, 2012.

Yu, S., Eder, B., Dennis, R., Chu, S.-H., and Schwartz, S. E.: New unbiased symmetric metrics for evaluation of air quality models, Atmospheric Science Letters, 7, 26–34, https://doi.org/10.1002/ASL.125, 2006.

Zhang, K., O'Donnell, D., Kazil, J., Stier, P., Kinne, S., Lohmann, U., Ferrachat, S., Croft, B., Quaas, J., Wan, H., Rast, S., and Feichter, J.: The global aerosol-climate model ECHAM-HAM, version 2: sensitivity to improvements in process representations, Atmos. Chem. Phys, 12, 8911–8949, https://doi.org/10.5194/acp-12-8911-2012, 2012.

Zhang, K., Wan, H., Liu, X., Ghan, S. J., Kooperman, G. J., Ma, P. L., Rasch, P. J., Neubauer, D., and Lohmann, U.: Technical note: On the use of nudging for aerosol-climate model intercomparison studies, Atmos. Chem. Phys., 14, 8631–8645, https://doi.org/10.5194/ACP-14-8631-2014, 2014.

Zoëga, T., Storelvmo, T., and Krüger, K.: Arctic warming from a high-latitude effusive volcanic eruption, Scientific Reports 2025 15:1, 15, 14653-, https://doi.org/10.1038/s41598-025-98811-5, 2025a.

Zoëga, T., Storelvmo, T., and Krüger, K.: Modelled surface climate response to effusive Icelandic volcanic eruptions: sensitivity to season and size, Atmos. Chem. Phys., 25, 2989–3010, https://doi.org/10.5194/ACP-25-2989-2025, 2025b.